KeA1

CHINESE ROOTS
GLOBAL IMPACT

Contents lists available at ScienceDirect

Petroleum Science

journal homepage: www.keaipublishing.com/en/journals/petroleum-science



Original Paper

Sedimentary paleoenvironment and its control on organic matter enrichment in the Mesoproterozoic hydrocarbon source rocks in the Ordos Basin, southern margin of the North China Craton



Zhi-Chen Wu a, b, Ju-Ye Shi a, b, *, Tai-Liang Fan a, b, Ming Jiang a, b

- ^a School of Energy Resources, China University of Geosciences (Beijing), Beijing, 100083, China
- ^b Key Laboratory of Marine Reservoir Evolution and Hydrocarbon Enrichment Mechanism, Ministry of Education, China University of Geosciences (Beijing), Beijing, 100083, China

ARTICLE INFO

Article history: Received 29 May 2023 Received in revised form 13 November 2023 Accepted 14 March 2024 Available online 15 March 2024

Edited by Jie Hao and Meng-Jiao Zhou

Keywords:
Cuizhuang formation
Paleoproterozoic source rocks
Marine productivity
Paleoenvironments
Submarine hydrothermal activity
Organic matter enrichment

ABSTRACT

The black shale of the Mesoproterozoic Cuizhuang Formation in the Changcheng System in Yongji city, North China Craton, is a potential source rock. Understanding the organic matter enrichment mechanism is crucial for evaluating source rock resources and understanding oil and gas accumulation mechanisms. In this study, we evaluated the sedimentary paleoenvironment and organic matter enrichment mechanisms of shale using thin section observations, mineral composition analysis, organic geochemistry, and elemental geochemistry. We found significant differences in the sedimentary paleoenvironment and organic matter enrichment mechanisms between the lower Cuizhuang Formation and the Beidajian Formation shale. The Cuizhuang Formation was deposited in a late-stage, restricted basin environment during the rift phase, and elemental and geochemical indicators showed that the Cuizhuang Formation was in a suboxic—anoxic water environment, that was influenced by a warm and humid paleoclimate and submarine hydrothermal activities, which promoted the accumulation of organic matter. However, the enrichment of organic matter in the Cuizhuang Formation was mainly controlled by redox conditions. The formation of suboxic-anoxic water environments may be closely related to the warm and humid paleoclimate and submarine hydrothermal activities. Warm conditions promote continental weathering and increase marine productivity, thereby consuming oxygen in the bottom water. Moreover, acidic hydrothermal activity also helps to establish an anoxic environment. Our results reveal the effects controlling various coupled mechanisms dominated by redox conditions, which may explain the development of source rocks in the Cuizhuang Formation.

© 2024 The Authors. Publishing services by Elsevier B.V. on behalf of KeAi Communications Co. Ltd. This is an open access article under the CC BY-NC-ND license (http://creativecommons.org/licenses/by-nc-nd/4.0/).

1. Introduction

The conventional belief disregarded the possibility of hydrocarbon accumulations within basins, geosynclines, and platforms hosting sedimentary rocks of Infracambrian or Precambrian age. The primary argument among petroleum geologists was the absence of life forms predating the Palaeozoic Era in these Infracambrian stratigraphic columns, leading to the rejection of Precambrian terranes (Dickas, 1986). However, with the continuous development of exploration theory and technological advances

E-mail address: shijuye@cugb.edu.cn (J.-Y. Shi).

(Wang et al., 2019, Wang et al., 2020a), searching for oil and gas resources in deeper and older strata has become a crucial goal for global exploration (Wang et al., 2022a; Jin, 2023). In fact, the discovery of deep-time oil and gas resources from Mesoproterozoic strata has been reported worldwide, including in Siberia, India, Western Africa, Australia, Canada, South America and cratons in other part of the world (Fowler and Douglas, 1987; Kuznetsov, 1997; Bazhenova et al., 1994; Galushkin et al., 2004). Oil and gas geological exploration and source research in the Mesoproterozoic to Neoproterozoic Yanliao Basin in North China are representative of Chinese early research on petroleum geology of ancient strata. These studies have confirmed the existence of Chinese ancient Proterozoic primary petroleum, and have discovered and demonstrated the formation of ancient oil reservoirs in the Proterozoic

^{*} Corresponding author. School of Energy Resources, China University of Geosciences (Beijing), Beijing, 100083, China.

period (Shi et al., 2008; Qin et al., 2010; Wang and Han, 2011; Luo et al., 2013). Hence, the deep-time oil and gas resources from Mesoproterozoic and Neoproterozoic to lower Cambrian strata hold significant energy potential and merit attention.

Organic-rich shale has been the focus of exploration and academic attention for many years for two primary reasons (Feng et al., 2020). First, mudstones with a high organic content provide valuable information about ancient oceans and serve as sensitive indicators of changes in paleoclimates and paleoenvironments (Goldberg and Humayun, 2010). Second, understanding the patterns of organic matter enrichment is crucial for guiding oil and gas exploration and identifying potential hydrocarbon resources. The debate over the productivity and preservation models of the mechanism of organic matter enrichment has been ongoing due to the complex physical and chemical processes involved in the accumulation of organic matter. While the preservation model emphasizes that low oxygen levels are conducive to the preservation of organic matter (Goodarzi et al., 2021), the productivity model asserts that abundant organic matter sedimentation dominates the accumulation of organic matter (Bechtel et al., 2012). However, neither model can fully explain the laws of organic matter enrichment. Studies have shown that control by a single factor is insufficient to explain the accumulation of organic matter in sediments. The mechanisms of organic matter accumulation in different basins must consider specific sedimentary environmental factors as the enrichment of organic matter may result from the coupling of multiple factors (Xu et al., 2015, 2021; Liu et al., 2019, 2021: Song et al., 2019).

The southern margin of the Ordos Basin, which is situated in the southern part of the North China Craton, comprises a middle Paleozoic rift basin that includes the Qin-Qi Sea and Xiong'er Rift. The Mesoproterozoic Changcheng System in the Ordos Basin is an area that has received relatively little attention due to its age and highly evolved nature. Previous research has primarily focused on the Paleozoic rift and sedimentary processes (Chen et al., 2016), geochemical characteristics of source rocks (Wang et al., 2018), distribution and exploration potential (Zhao et al., 2018), exploration prospects, and evolution of biota (Meng et al., 2005; Hao et al., 2016). The Cuizhuang Formation (1647.8 \pm 4.3 Ma; Lyu et al., 2022), which is part of the Changcheng System, is a significant stratigraphic unit that contains abundant organic-rich shale. The Cuizhuang Formation stands as the sole occurrence of Mesoproterozoic black shale within the Xiong'er Basin as well as the Ordos Basin, and is garnering escalating attention as a prospective source rock (Pan et al., 2020; Khaled et al., 2022). Comprehending the factors governing organic matter accumulation in the Cuizhuang Formation is crucial in assessing the potential for deep oil and gas resources in the southern margin of the Ordos Basin. However, the mechanism of organic matter enrichment in the Cuizhuang Formation is still poorly understood. Previous studies have revealed that the shale in the Cuizhuang Formation is primarily composed of clay minerals and quartz, with high thermal maturity, making it a valuable source rock for oil and gas (Khaled et al., 2022). There are currently models, as outlined by Wang et al. (2022b), that demonstrate broad effectiveness in evaluating highly mature marine source rocks across deep basins worldwide. The sedimentary environment of the Cuizhuang Formation shale was an anoxic submarine passive continental margin (Pan et al., 2020). Additionally, the carbonate rocks of the Luoyu Group contain asphalt filling and macroscopic dissolution pores, which make them effective reservoirs. The Cambrian mudstone, sandstone, and mudstone carbonate rocks overlying the Luoyu Group can serve as effective cap rocks, forming a potential combined reservoir of the Changcheng System and the underlying hydrocarbon source rocks and Luoyu Group reservoirs (Wang et al., 2018). Therefore, further research is required to

comprehensively investigate the mechanisms of organic matter enrichment in the Cuizhuang Formation.

However, it is crucial to study the potential high-quality source rocks in the Paleoproterozoic strata to promote deep and ultradeep oil and gas exploration in the North China Craton. The goal of this study is to analyze various lithological samples from the Paleoproterozoic Changcheng System of to elucidate the role of marine productivity and redox conditions in the accumulation and preservation of organic matter. This goal is achieved by examining total organic carbon (TOC) and stable carbon isotopes, as well as major, trace, and rare earth elements. Furthermore, this research emphasizes the potential impact of climate change and submarine hydrothermal activity on organic matter accumulation and preservation in the Cuizhuang Formation in the Changcheng System.

2. Regional geologic background

The evolution of Chinese marine sedimentary basins is influenced by the dispersal, convergence, and rotation of global supercontinents. This evolution has resulted in several periods of cratonic rifting and sag basin formation that provide important structural backgrounds for the formation of ultradeep oil and gas geological conditions (Wang and Li, 2003; Zhai, 2013). The major Chinese cratonic plates include the Yangtze, North China, and Tarim plates. Among them, the North China Craton was affected by the breakup of the Columbia supercontinent in the early Mesoproterozoic (approximately 1.8–1.3 Ga) and underwent regional rifting, leading to the formation of four major rifts, including the Xiong'er rift, Zhaertai-Baiyun'ebo rift, Ordos rift, and Yanshan-Liaoning rift (Zhao et al., 2002). The formation of these rifts controls the distribution of the source rocks in the Changcheng System. Notably, the Changcheng System, dating back approximately 1.8-1.4 Ga, differs by a significant 200 Ma from the international boundary of 1.6 Ga that separates the Paleoproterozoic and Mesoproterozoic eras. In the North China Craton, the "Lüliang movement" is recognized as a significant thermal event that marked the formation of the crystalline basement. Subsequently, the Changcheng System developed as a prominent representative of platform-type sedimentary cover layers. The Chinese geological community has long considered the sedimentation of the Changcheng System as the beginning of the Mesoproterozoic era, placing the boundary between the Paleoproterozoic and Mesoproterozoic eras at 1.8 Ga, deviating by 200 Ma from the international stratigraphic chart.

During the initial phase of the Changcheng System formation, the southern margin of the North China Plate was situated in a passive continental margin tectonic setting. As the Xiong'er rift continued to extend and fault, a continental-oceanic environment formed in the southern margin of the Ordos Basin, and the sedimentary stage began. Initially, sedimentation was dominated by terrestrial deltas, while in the later stage, as the relative sea level increased, sedimentation was characterized by littoral and shallow marine facies. The filling process can be divided into four stages (Deng et al., 2021)(Fig. 1c).

(1) Beginning of the rifting and initial filling of the Xiong'er Basin (1.80–1.75 Ga)

The Xiong'er Group in the Xiong'er Basin experienced terrestrial to marine depositional transitions due to rift magmatism. Sediments infilled the basin in a triangular shape, bounded by fault zones. Volcanic magmatism extended to the Ordos Basin, forming the Guyuan rift (Li et al., 2019). In the north, the initial transgressive sediments of the Changcheng System begun to deposit (Zhong, 2015).



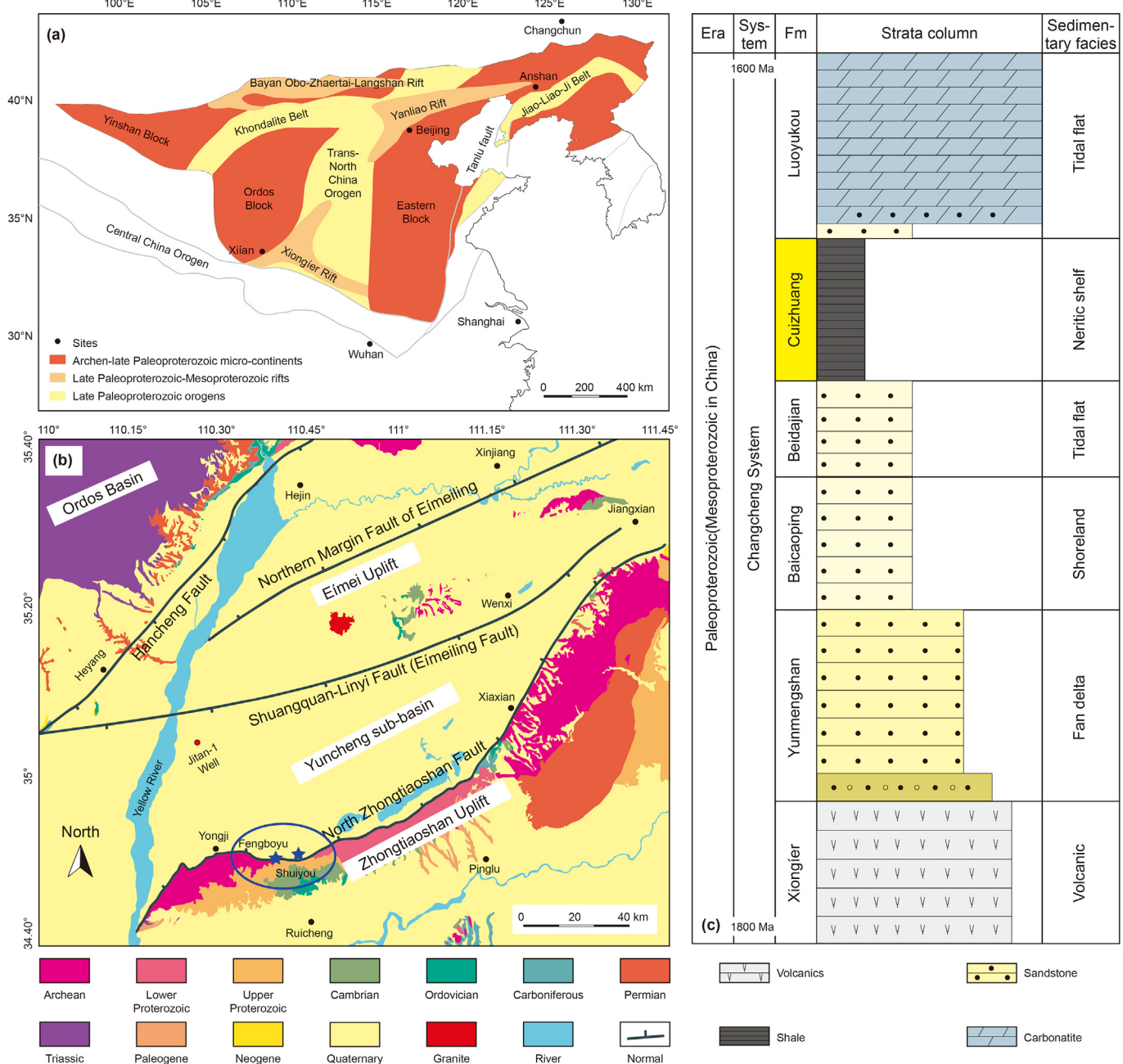


Fig. 1. (a) Paleoproterozoic tectonic map of the North China Craton, modified from Zhao et al. (2002). (b) The Yuncheng Basin simplified geological map, modified from Khaled et al. (2022). The location of Fengboyu and Shuiyou profiles was marked with blue pentagram. (c) Depositional filling processes of the Xiong'er rift Changcheng System.

(2) Initial transgressive overlap from south to north (1.75–1.70 Ga)

After the Xiong'er Group deposition, the southern margin of the North China Craton uplifted briefly, then subsided. Transgression occurred in the south, depositing littoral clastic rocks (Gaoshanhe Group). Simultaneously, the Bingmagou Formation formed alluvial fan-delta-fluvial deposits in northern elevated areas, transitioning to coastal facies due to gradual transgression (Meng et al., 2018).

(3) Large-scale transgressive overlap within the Taihang Mountain area $(1.70-1.65\ \text{Ga})$

During the extensive transgression, the Yunmengshan and

Baicaoping formations in the Xiong'er Basin were deposited as sandstones and mudstones in the tidal flat-neritic facies (Qiao and Wang, 2014).

(4) The most extensive Changchen System transgressive deposition in NCC (1.65–1.60 Ga)

During this period, the Xiong'er Basin and Yanliao Basin potentially connected via the Taihang Mountain area, leading to extensive deposition in the North China Craton (NCC). The depositional environments in both basins shifted from deep-water shelf facies to littoral-neritic sea-tidal flat facies.

This study focuses on the Cuizhuang Formation and Beidajian Formation shale of the Changcheng System which are well exposed

in the Zhongtiao Mountains of Yongji city, Shanxi Province.

3. Methods

3.1. Samples and analytical method

In this study, 104 fresh rock samples of various lithologies were collected from the Fengboyu (34°49′4″N, 110°39′22″E) and Shuiyou (34°49′53″N, 110°44′9″E) sections in the Zhongtiao Mountains of North China (Yongji city, Shanxi Province, Fig. 1). To avoid sample contamination, 14 and 13 samples were selected from the Fengboyu and Shuiyou sections, respectively, after removing weathered surfaces, and were analyzed for total organic carbon (TOC), major and trace elements. All analyses were conducted at the China National Nuclear Corporation (CNNC).

TOC values were measured using a CS-400 carbon—sulfur analyzer from LECO Corporation in the United States. Samples were treated with dilute hydrochloric acid to remove inorganic carbon before being combusted via high-temperature oxygen flow. The resulting carbon dioxide was then quantified using an infrared detector to calculate the TOC content of each sample.

The mineral composition was analyzed using a Panalytical X' Pert PRO X-ray diffractometer. The sample was crushed and placed on a copper holder for analysis using CuK α radiation. The instrument has an analytical accuracy better than 0.02%, ensuring the accuracy of the results.

Major element analysis was performed using an AB104L, Axios—mAX wavelength dispersive X-ray fluorescence spectrometer. The samples were ashed at $1000\,^{\circ}\text{C}$ for 90 min and mixed with $\text{Li}_2\text{B}_4\text{O}_7$ before being melted into glass beads for analysis. The instrument precision is within 1%-5%.

Trace elements and rare earth elements were measured using an ELEMENT XR inductively coupled plasma mass spectrometry (ICP–MS) instrument. Fifty milligrams of sample was dissolved in a mixture of hydrofluoric acid (HF) and nitric acid (HNO₃). The resulting solution was evaporated to near dryness, redissolved, and diluted to 100 g with a 2% HNO₃ mixture before analysis by ICP–MS. Precision and accuracy were evaluated by repeated analyses of the sample and three international reference standards (BCR-2, BHVO-2, and GSR-6). The precision of the trace element concentration analysis was better than ±5%.

3.2. Data presentation

The enrichment factor ($X_{\rm EF}$) is commonly utilized to describe the degree of element enrichment in sediments (Tribovillard et al., 2006). To further assess the paleoredox state, we introduced an enrichment factor to quantify the degree of enrichment or depletion of trace elements. We calculated the $X_{\rm EF}$ using the following formula:

$$X_{EF} = (X / Al)_{sample} / (X / Al)_{PAAS}$$
 (1)

Here, X denotes the concentration of the element normalized to post—Archean average shale (PAAS) (Pourmand et al., 2012). $X_{\rm EF}$ values >1.0 or <1.0 signify element enrichment or depletion in sediments, respectively.

Enriched trace elements in sediments can be attributed to authigenic deposition, terrigenous input, and hydrothermal sedimentation. To accurately recover the paleoproductivity level, it is crucial to eliminate the terrigenous residual component of P and Ba. Using Al as a standard can mitigate the impact of terrigenous input, as it is less susceptible to weathering and post-sedimentation

changes (Tribovillard et al., 2006; Algeo and Rowe, 2012). To evaluate the paleoproductivity level, the content of organic phosphorus (P_{org}) and biogenic Ba (Ba_{bio}) can be quantified using the following formula (Schoepfer et al., 2015; Dong et al., 2017):

$$P_{org} = P_{tot} - Al \times (P/Al)_{detr}$$
 (2)

$$Ba_{bio} = Ba_{tot} - Al \times (Ba/Al)_{detr}$$
(3)

Here, (P/Al)_{detr} and (Ba/Al)_{detr} signifies the average ratio in crustal rocks (Shen et al., 2015; He et al., 2020). Paleoproductivity levels can be classified as high, medium, or low based on Ba_{bio} values greater than $1000 \, \mu g/g$, between $200 \, and \, 1000 \, \mu g/g$, and less than $200 \, \mu g/g$, respectively (Murray and Leinen, 1993).

The chemical index of alteration (CIA) is a widely-used proxy for assessing soil and sediment chemical weathering and its relevance to paleoclimate reconstruction. It was initially proposed by Nesbitt and Young in 1982 and has been explored in various studies (Fedo et al., 1995; Wang et al., 2020b). CIA values are influenced by the removal of mobile cations during chemical weathering, which is more pronounced under warmer and wetter climate conditions. The calculation for CIA is as follows:

$$CIA = [Al_2O_3 / (Al_2O_3 + CaO^* + Na_2O + K_2O)] \times 100$$
 (4)

To calculate CIA, the molar units of all oxides are considered. CaO* specifically represents CaO in the silicate fraction, excluding its presence in apatite and carbonate. A correction procedure for CaO* follows McLennan's method (1993): (1) CaO is initially adjusted for its contribution from apatite using P_2O_5 data $(\text{CaO}' = \text{CaO} - 10/3 \times P_2O_5)$. (2) If CaO' is greater than Na2O, the final CaO* value is set as Na2O. Conversely, if CaO' is less than Na2O, the final CaO* value is set as CaO'.

4. Results

Table 1 presents the analytical results of the TOC, major and trace elements of rock samples obtained from the Cuizhuang Formation and Beidajian Formation. Table 2 presents mineralogical composition of the Cuizhuang Formation and Beidajian Formation. The results of the rare earth element analysis are summarized in Table 3, while Table 4 displays the calculated parameters of major elements, trace elements, and rare earth elements.

4.1. Lithology and mineral analysis

The mineral composition of the study area was analyzed using X-ray diffraction (XRD), revealing that the dominant minerals included clay minerals, quartz, K-feldspar, and calcite, as well as small amounts of siderite, pyrite, and hematite. As shown in Table 2, the lower part of the Cuizhuang Formation in the Fengboyu section had an average clay mineral content of 53.8 wt% (ranging from 66.0 wt% to 15.8 wt%), while the Beidajian Formation at the Shuiyou section had an average content of 56.2 wt% (ranging from 68.9 wt% to 38.8 wt%). The quartz content varied greatly, ranging from 76.0 wt% to 21.0 wt% (average of 35.5 wt%) in the lower part of the Cuizhuang Formation and from 39.8 wt% to 10.3 wt% (average of 21.2 wt%) in the Beidajian Formation. The K-feldspar content was low, with an average of 4.2 wt% in the lower part of the Cuizhuang Formation and an average of 13.0 wt% in the Beidajian Formation. The Calcite content was also low, with an average of 8.0 wt%, and the contents of other minerals were relatively stable and low. The Cuizhuang Formation shale exhibited a mudstone texture under the microscope, and the mudstone was mainly composed of quartz

Table 1TOC, the major and trace elements of Mesoproterozoic Cuizhuang and Beidajian sediments in North China.

Sample	Lithology	TOC, %	Major elements, %										Trace element, ppm							
			Si	Al	Fe	Mg	Ca	Na	K	Mn	Ti	P	Мо	U	V	Cr	Ba	Rb	Sr	
FBY-1	Black shale	0.093	28.76	9.20	2.60	1.39	0.83	0.10	5.71	0.01	0.46	0.04	0.18	2.42	63.60	118.00	368.00	196.00	83.50	
FBY-3	Gray shale	0.129	28.04	9.17	3.02	1.48	0.95	0.04	5.80	0.04	0.47	0.04	0.21	1.74	76.70	129.00	366.00	203.00	119.00	
FBY-5	Black sandy shale	0.106	30.72	6.00	5.20	1.35	0.67	0.01	3.92	0.12	0.49	0.03	0.27	1.24	85.40	111.00	341.00	132.00	73.20	
FBY-6	Black sandy shale	0.131	38.30	2.67	2.86	0.68	0.79	0.03	1.76	0.08	0.16	0.01	0.49	0.98	26.00	130.00	3354.0	61.00	89.10	
FBY-8	Black shale	0.887	25.35	7.65	7.84	1.53	0.24	0.03	5.19	0.16	0.69	0.02	0.88	1.40	92.30	123.00	312.00	143.00	69.10	
FBY-10	Black shale	0	20.07	6.38	13.69	2.37	0.36	0.02	4.10	0.25	0.49	0.02	0.26	0.95	87.50	94.70	182.00	119.00	53.70	
FBY-13	Black shale	0.302	27.74	9.15	3.98	1.42	0.21	0.04	5.86	0.03	0.71	0.03	0.32	1.13	105.00	80.40	251.00	173.00	67.30	
FBY-14	Black shale	0.268	26.95	9.42	4.12	1.50	0.69	0.05	5.62	0.03	0.72	0.03	0.27	1.17	129.00	110.00	202.00	183.00	60.70	
FBY-16	Black shale	0.171	28.35	9.46	2.84	1.33	0.20	0.04	5.76	0.01	0.82	0.03	0.17	0.99	137.00	84.30	177.00	173.00	66.20	
FBY-17	Black shale	0.212	29.24	8.64	3.14	1.22	0.25	0.05	5.58	0.01	0.74	0.02	0.20	1.35	139.00	126.00	311.00	154.00	93.30	
FBY-19	Black shale	0.538	29.62	9.00	2.69	1.22	0.18	0.02	5.28	0.01	0.68	0.02	0.31	1.22	151.00	111.00	215.00	178.00	88.10	
FBY-22	Black shale	0.533	29.50	7.87	4.29	1.21	0.14	0.03	5.06	0.02	0.61	0.02	0.40	1.35	131.00	106.00	267.00	159.00	64.70	
FBY-24	Black shale	0.590	30.67	8.32	2.42	1.15	0.18	0.02	5.08	0.01	0.68	0.02	0.24	1.28	178.00	122.00	198.00	174.00	75.50	
FBY-26	Black shale	0.757	27.78	8.44	4.89	1.47	0.20	0.03	5.09	0.02	0.64	0.02	0.41	1.40	160.00	76.80	183.00	208.00	79.10	
SY-1	Gray green shale	0.073	27.88	10.64	1.53	0.92	0.41	0.08	8.61	0.00	0.55	0.11	0.18	1.86	105.00	65.40	696.00	201.00	145.00	
SY-5	Gray green shale	0.107	28.53	9.39	1.73	0.89	1.14	0.12	7.91	0.01	0.62	0.21	0.42	2.54	113.00	65.70	684.00	200.00	134.00	
SY-8	Black shale	0.188	27.54	9.70	1.61	0.89	1.75	0.08	8.21	0.01	0.49	0.14	0.57	2.78	109.00	28.20	614.00	174.00	132.00	
SY-9	Black shale	0.194	25.92	11.70	1.74	1.16	0.55	0.07	8.75	0.00	0.65	0.11	0.39	2.44	125.00	76.50	1268.0	222.00	145.00	
SY-14	Gray shale	0.144	24.15	10.45	2.75	1.76	1.83	0.05	7.34	0.01	0.53	0.09	0.35	2.93	110.00	72.10	580.00	240.00	165.00	
SY-17	Gray shale	0.062	28.62	8.97	2.79	1.30	0.62	0.06	7.50	0.00	0.49	0.08	0.20	1.66	86.50	102.00	632.00	213.00	115.00	
SY-21	Purple sandy shale	0.027	29.71	7.73	4.47	1.07	0.61	0.08	6.65	0.01	0.36	0.09	0.47	3.47	103.00	124.00	1141.00	194.00	164.00	
SY-25	Gray green shale	0.083	26.82	9.36	3.01	1.72	1.54	0.06	7.23	0.01	0.48	0.10	0.19	5.21	97.10	126.00	668.00	246.00	156.00	
SY-26	Gray shale	0.079	27.68	10.06	2.62	1.31	0.59	0.09	7.65	0.01	0.50	0.12	0.40	4.98	92.40	122.00	807.00	226.00	163.00	
SY-29	Gray shale	0.138	25.12	11.29	2.72	1.51	1.09	0.04	7.67	0.01	0.48	0.11	0.23	4.71	144.00	153.00	557.00	250.00	152.00	
SY-31	Black shale	0.193	26.73	11.26	1.79	1.16	0.47	0.05	8.40	0.00	0.47	0.09	0.20	5.66	116.00	102.00	486.00	254.00	130.00	
SY-33	Black sandy shale	0.215	28.05	10.18	1.69	0.85	0.48	0.09	9.01	0.01	0.54	0.13	0.58	2.19	101.00	80.80	771.00	203.00	172.00	
SY-34	Gray sandy shale	0.125	27.72	10.27	1.97	0.91	0.53	0.08	8.82	0.01	0.56	0.11	0.41	2.11	115.00	74.50	602.00	232.00	142.00	
UCC		1	30.80	8.15	3.53	1.49	2.56	2.43	2.32	0.08	0.38	0.07	1.50	2.80	60.00	35.00	550.00	112.00	350.00	

 Table 2

 Mineralogical composition of Mesoproterozoic Cuizhuang and Beidajian sediments in North China ("/" indicates not detected due to low levels).

Sample	Lithofacies	Mineral co	Mineral composition, wt%												
		Quartz	K-feldspar	Clays	Calcite	Siderite	Pyrite	Hematite							
FBY-1	Siliceous-rich argillaceous shale	33.2	4.1	57.5	5.2		1								
FBY-3	Siliceous-rich argillaceous shale	27.9	4.5	60.6	7	1	1	1							
FBY-6	Siliceous shale	76	3.2	15.8	5	1	1	1							
FBY-8	Siliceous shale	32.5	5.7	47.4	1	14.3	1	1							
FBY-10	Argillaceous/siliceous mixed shale	21	2.6	46.7	1	29.7	1	1							
FBY-13	Argillaceous-rich siliceous shale	28.7	4.8	58.7	7.8	1	1	1							
FBY-14	Siliceous-rich argillaceous shale	26.1	3.3	66	4.6	1	1	1							
FBY-17	Argillaceous-rich siliceous shale	36.3	6	57.6	1	1	1	1							
FBY-19	Siliceous-rich argillaceous shale	31.4	5.3	63.3	1	ĺ	1	1							
FBY-22	Argillaceous-rich siliceous shale	41.7	5.1	53.2	1	1	1	1							
FBY-24	Argillaceous/siliceous mixed shale	40.5	3.2	56.3	1	1	1	1							
FBY-26	Argillaceous/siliceous mixed shale	30.5	2.9	62.4	1	1	4.1	1							
SY-1	Siliceous-rich argillaceous shale	15.5	14.3	55.9	14.3	1	1	1							
SY-5	Argillaceous/siliceous mixed shale	29.7	11.5	49.5	9.3	1	1	1							
SY-8	Argillaceous/siliceous mixed shale	25.2	17.1	46.9	10.8	1	1	1							
SY-9	Siliceous-rich argillaceous shale	10.3	18.8	64.4	6.6	1	1	1							
SY-14	Argillaceous/siliceous mixed shale	11.7	7.9	68.9	11.5	1	1	1							
SY-17	Argillaceous-rich siliceous shale	31.7	12.4	48.1	7.9	1	1	1							
SY-21	Argillaceous-rich siliceous shale	39.8	9.2	38.8	6.2	1	/	6							
SY-26	Siliceous-rich argillaceous shale	24.1	11.3	58.4	6.2	1	1	1							
SY-31	Siliceous-rich argillaceous shale	12.2	13.5	66.1	8.2	1	1	1							
SY-37	Siliceous-rich argillaceous shale	11.4	13.7	64.9	10.1	Ī	Ì	1							

and clay minerals. The quartz cement was widely distributed in the dark shale during the process of clay mineral transformation (Thyberg and Jahren, 2011; Milliken et al., 2012) (Fig. 2(e) and (f)).

4.2. Organic matter

The total organic carbon (TOC) content is a crucial parameter for evaluating the abundance of organic matter in sedimentary rocks. In the lower section of the Cuizhuang Formation, the TOC contents ranged from 0.093% to 2.16% (averaging 0.491%), while in the

Beidajian Formation, the contents ranged from 0.027% to 0.194% (averaging 0.125%), as shown in Table 1.

4.3. Elemental analyses

4.3.1. Major elements

The Si content was the highest among all analyzed samples, with an average of 27.98 wt% and a range of 20.07 wt% to 38.30 wt%. The next most abundant major elements were Al, K, and Fe, with average contents of 8.98 wt%, 6.43 wt%, and 3.48 wt%, respectively,

 Table 3

 The rare earth elements of Mesoproterozoic Cuizhuang sediments in North China.

Sample	Lithology	Rare elements, ppm														
		La	Ce	Pr	Nd	Sm	Eu	Gd	Tb	Dy	Но	Er	Tm	Yb	Lu	Y
FBY-5	Black sandy shale	29.7	59.1	7.48	30.6	5.28	1.13	4.75	0.845	4.09	0.813	2.4	0.367	2.35	0.348	21.3
FBY-8	Black shale	36.5	65.4	8.7	33.3	6	1.6	5.58	1	5.33	1.03	2.8	0.453	2.99	0.456	26.5
FBY-10	Black shale	25.5	46.9	6.27	24.7	4.68	1.13	4.26	0.715	3.85	0.786	2.31	0.336	2.22	0.345	18.5
FBY-13	Black shale	38.9	70.7	9.5	38.7	6.78	1.78	6.09	1.02	4.88	1.03	2.87	0.473	2.88	0.416	25.5
FBY-14	Black shale	33.4	63.7	8.44	33.9	5.6	1.61	5.54	1.08	5.88	1.27	3.35	0.539	3.44	0.529	33.4
FBY-16	Black shale	30.6	57.1	7.77	31.3	6.45	1.74	5.45	0.995	5.07	0.956	2.64	0.401	2.54	0.393	24.2
FBY-17	Black shale	27.4	56.4	7.39	30.8	5.33	1.53	4.82	0.869	4.25	0.826	2.31	0.374	2.53	0.347	21.7
FBY-19	Black shale	28.8	56.2	6.91	29.2	5.5	1.29	4.77	0.91	4.96	1.05	2.75	0.468	2.98	0.503	25.1
FBY-22	Black shale	36.3	63.3	8.78	33.5	6.06	1.45	5.38	1.01	5.12	0.903	2.72	0.435	2.93	0.407	25.3
FBY-24	Black shale	40.2	70.8	9.74	36.6	6.73	1.73	5.82	1.11	5.68	1.15	3.18	0.471	3.18	0.47	27.4
FBY-26	Black shale	36.6	65.2	9.19	37	6.49	1.52	5.8	1.09	5.5	1.14	3.26	0.514	3.35	0.481	29.9
PAAS		44.56	88.75	10.15	37.32	6.884	1.215	6.043	0.8914	5.325	1.052	3.075	0.451	3.012	0.4386	27.31

Abbreviation: PAAS = Post-Archean Australian Shales (Pourmand et al., 2012).

Table 4Major and trace element geochemical parameters of Mesoproterozoic Cuizhuang and Beidajian sediments in North China.

Sample	Lithology	P _{org} , ppm	Ba _{bio} , ppm	Mo _{EF}	U _{EF}	C _{org} /P _{tot}	Rb/Sr	CIA	Ba/Sr	Y/Ho	REE, μg/g	LREE, μg/g	HREE, μg/g	(Nd/Yb) _N	Eu/Eu*
FBY-1	Black shale	471.54	202.47	0.19	0.85	6.32	2.35	68.77	4.41	27.52	243.76	222.96	20.80	1.32	1.11
FBY-3	Gray shale	572.69	200.95	0.23	0.61	7.87	1.71	69.08	3.08	29.33	243.70	223.25	20.45	1.44	1.11
FBY-5	Black sandy shale	349.87	232.94	0.46	0.67	10.28	1.80	68.69	4.66	26.20	149.25	133.29	15.96	1.05	1.20
FBY-6	Black sandy shale	74.39	3305.97	1.84	1.18	40.79	0.68	67.36	37.64	28.65	43.78	36.62	7.16	0.51	0.53
FBY-8	Black shale	198.53	174.30	1.15	0.59	99.02	2.07	67.68	4.52	25.73	171.14	151.50	19.64	0.90	1.47
FBY-10	Black shale	213.58	67.17	0.40	0.48	260.82	2.22	68.93	3.39	23.54	124.00	109.18	14.82	0.90	1.34
FBY-13	Black shale	223.61	86.33	0.34	0.40	28.82	2.57	68.81	3.73	24.76	186.02	166.36	19.66	1.08	1.47
FBY-14	Black shale	211.68	32.38	0.28	0.40	25.58	3.01	70.28	3.33	26.30	168.28	146.65	21.63	0.80	1.53
FBY-16	Black shale	280.07	6.71	0.17	0.34	14.66	2.61	69.92	2.67	25.31	153.41	134.96	18.45	0.99	1.56
FBY-17	Black shale	65.63	155.48	0.23	0.50	28.51	1.65	68.59	3.33	26.27	145.18	128.85	16.33	0.98	1.60
FBY-19	Black shale	/	53.00	0.34	0.44	81.62	2.02	70.93	2.44	23.90	146.29	127.90	18.39	0.79	1.34
FBY-22	Black shale	69.12	125.39	0.51	0.55	76.92	2.46	68.80	4.13	28.02	168.30	149.39	18.91	0.92	1.35
FBY-24	Black shale	59.39	48.20	0.28	0.50	83.12	2.30	70.13	2.62	23.83	186.86	165.80	21.06	0.93	1.47
FBY-26	Black shale	24.12	31.01	0.48	0.54	114.84	2.63	70.19	2.31	26.23	177.14	156.00	21.14	0.89	1.32
SY-1	Gray green shale	478.38	238.43	0.17	0.56	1.71	1.39	63.43	4.80	26.40	299.35	280.21	19.14	1.75	1.15
SY-5	Gray green shale	2969.27	280.15	0.45	0.87	1.32	1.49	62.10	5.10	26.95	251.52	229.42	22.10	1.34	1.41
SY-8	Black shale	1359.05	196.72	0.59	0.92	3.44	1.32	62.39	4.65	26.50	228.86	210.29	18.57	1.17	1.25
SY-9	Black shale	234.24	764.90	0.33	0.67	4.61	1.53	65.35	8.74	28.16	279.61	259.34	20.27	1.48	1.11
SY-14	Gray shale	55.13	130.62	0.33	0.90	4.12	1.45	66.86	3.52	27.11	363.77	336.78	26.99	1.50	1.16
SY-17	Gray shale	59.90	246.14	0.23	0.60	2.05	1.85	62.73	5.50	29.45	168.28	155.32	12.96	1.45	1.35
SY-21	Purple sandy shale	599.77	808.64	0.61	1.45	0.76	1.18	61.79	6.96	28.29	152.67	137.60	15.07	1.12	1.39
SY-25	Gray green shale	505.39	265.52	0.20	1.80	2.13	1.58	64.56	4.28	27.95	241.04	222.39	18.65	1.68	1.26
SY-26	Gray shale	730.66	374.47	0.39	1.60	1.75	1.39	64.70	4.95	27.59	260.66	244.56	16.10	2.02	1.23
SY-29	Gray shale	253.86	71.66	0.21	1.35	3.36	1.64	67.64	3.66	26.06	423.06	396.28	26.78	1.76	1.19
SY-31	Black shale	/	2.02	0.18	1.62	5.26	1.95	65.58	3.74	28.16	356.97	331.13	25.84	1.68	1.10
SY-33	Black sandy shale	1048.20	333.46	0.57	0.69	4.23	1.18	61.22	4.48	29.67	281.54	262.45	19.09	1.93	1.22
SY-34	Gray sandy shale	519.83	160.36	0.40	0.66	2.96	1.63	62.10	4.24	30.18	304.89	285.35	19.54	1.73	1.31

and ranges of 2.67–11.70 wt%, 1.76–9.01 wt%, and 1.53–13.69 wt%, respectively. Compared with the upper continental crust (UCC) (McLennan, 2001), the analyzed samples of the lower part of the Cuizhuang Formation had higher average contents of Fe, Mg, K, and Ti, and lower average contents of Si, Al, Ca, Na, Mn, and P. The analyzed samples of the Beidajian Formation had higher average contents of Al, K, Ti, and P, and lower average contents of Si, Fe, Mg, Ca, Na, and Mn.

4.3.2. Trace elements

Table 1 presents the results of trace element analysis. The samples from the lower section of the Cuizhuang Formation exhibited enrichment in the redox-sensitive trace elements V and Cr (Vanschmus, 1986), with V concentrations ranging from 26 to 178 ppm (mean = 112 ppm) and Cr concentrations ranging from 77 to 130 ppm (mean = 109 ppm) relative to the UCC. Conversely, Ba (mean = 481 ppm), Mo (mean = 0.33 ppm), U (mean = 1.33 ppm), and Sr (mean = 142 ppm) exhibited lower concentrations compared to the UCC. Furthermore, Rb was significantly enriched,

with an average value of 161 ppm. The samples from the Beidajian Formation also demonstrated enrichment in redox-sensitive trace elements V (mean = 109 ppm), Cr (mean = 92 ppm), and U (mean = 3.27 ppm). Conversely, Mo (mean = 0.35 ppm) and Sr (mean = 77 ppm) exhibited lower concentrations relative to the UCC. Rb was also significantly enriched, with an average value of 220 ppm.

4.3.3. Rare earth elements

Table 3 presents the concentrations of rare earth elements (REEs) in the Cuizhuang Formation samples, which ranged from 44 to 244 ppm (average = 165 ppm). The concentration is higher than that of the upper continental crust (UCC) but lower than that of the Australian Proterozoic shale. Light REEs (LREEs) such as La, Ce, Pr, Nd, Sm, and Eu, accounted for 88.97% of the total REEs, with a total concentration (Σ LREE) ranging from 37 to 223 ppm (average = 147 ppm). In contrast, heavy REEs (HREEs) such as Gd, Tb, Dy, Ho, Er, Tm, Yb, and Lu, account for 11.03% of the total REEs, with a total concentration (Σ HREE) ranging from 7 to 22 ppm

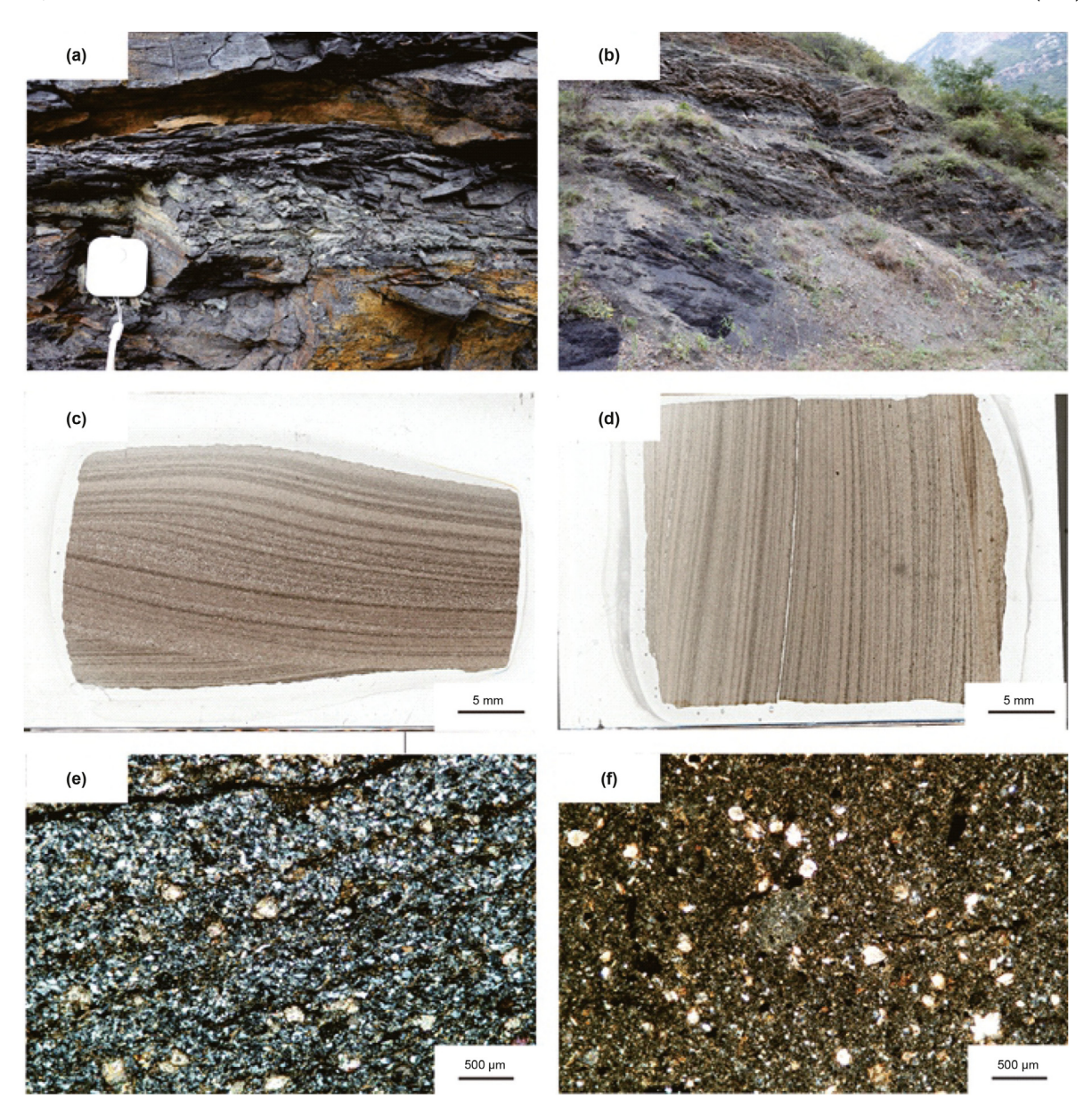


Fig. 2. Lithology characteristics of the section of the Cuizhuang and Beidajian Formation shale. (a) and (b) show the section of the Cuizhuang Formation shale with blocky texture. (c) and (d) show the section of the Beidajian Formation shale with horizontal bedding and wavy bedding. (e) and (f) are the thin sections showing the clay and quartz cement are dominated and widely distributed in the dark shale matrix.

(average = 18 ppm) (Taylor and Mclennan, 1985). These results suggest LREE enrichment and HREE depletion in the Cuizhuang Formation samples. In comparison, the average REE concentration of the Beidajian Formation samples is 278 ppm, which is higher than that of the PAAS, with an average $\Sigma LREE$ of 258 ppm, accounting for 92.77% of the total REEs. The average $\Sigma HREE$ was 20 ppm, accounting for 7.23% of the total REEs, indicating a similar pattern of LREE enrichment and HREE depletion.

5. Discussion

5.1. Lithological characterization

This study quantitatively analyzed the whole—rock mineral composition to classify rocks using a petrological naming method based on carbonate minerals, feldspathic minerals, and clay

minerals as endmembers. A ternary diagram method was employed for two-level rock naming. Four primary lithofacies zones were identified using the 50% boundary as the main rock name criterion. These four primary zones were further subdivided into 12 secondary lithofacies zones using a mineral content boundary of 25%. Based on mineral content, the samples were classified into four lithologies, namely: siliceous shale (S), argillaceous-rich siliceous shale (ASM), and siliceous-rich argillaceous shale (SA), as shown in Fig. 3.

The lower section of the Cuizhuang Formation is characterized by two organic-rich lithofacies composed of gray—black to black shales and siltstones, while the top of the underlying Beidajian Formation consists of gray to gray—green shales and sandstones with low organic content. The lower section of the Cuizhuang Formation exhibits a blocky texture indicative of deposition in a

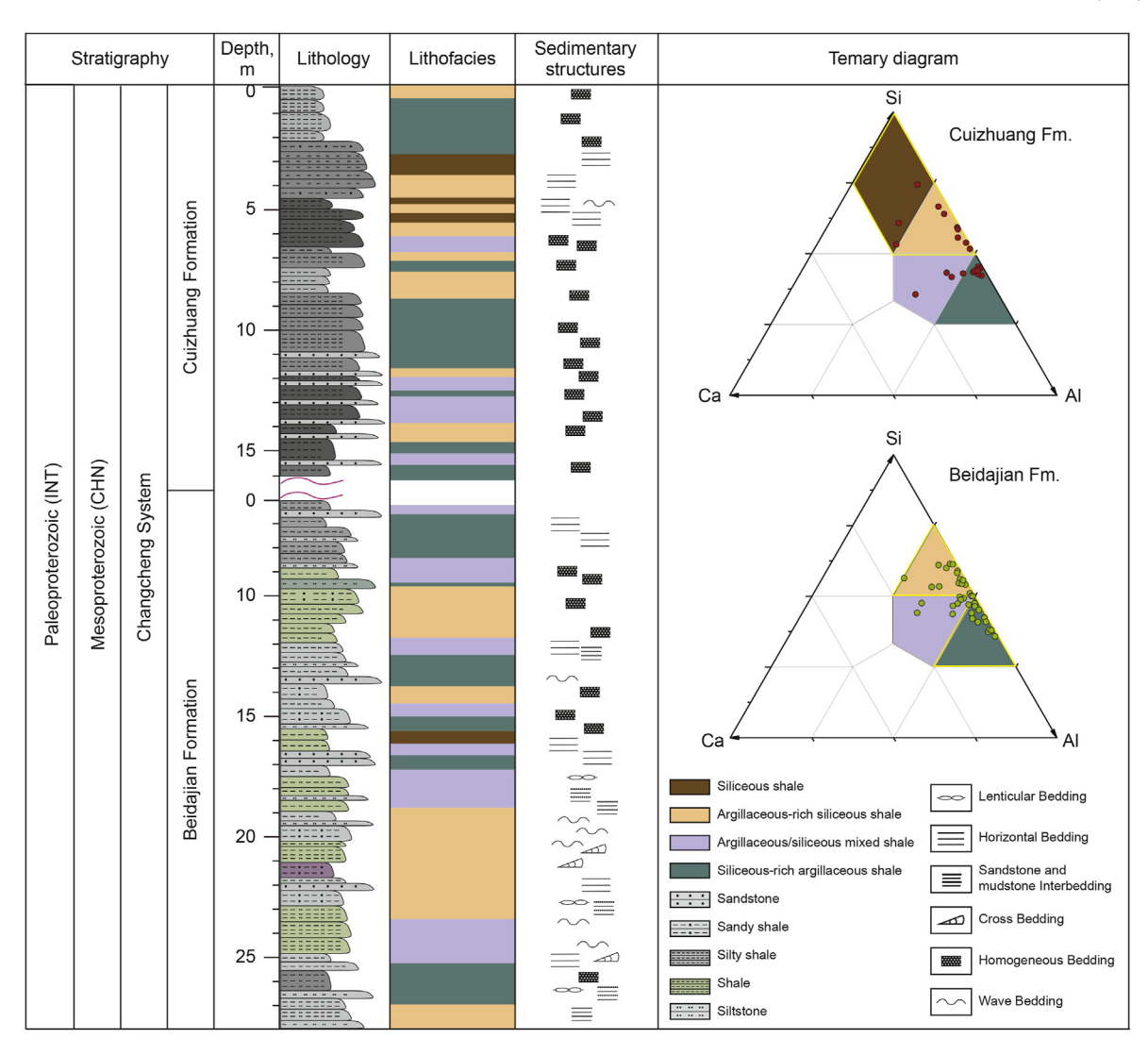


Fig. 3. Lithology, Lithofacies, and sedimentary structures of Cuizhuang Formation and Beidajian Formation. Ternary diagram shows the mineralogic composition of four major lithofacies from Cuizhuang to Beidajian formations in the Mt.Zhongtiao area.

shallow marine shelf environment (Fig. 2(a) and (b)). Conversely, the Beidajian Formation shows predominantly horizontal and wavy tidal bedding indicative of a subtidal to intertidal depositional environment (Fig. 2(c) and (d)).

5.2. Marine productivity

Nutrient-rich conditions in the ocean can stimulate mass reproduction of organisms, leading to increased organic productivity and subsequent accumulation of organic matter (Tribovillard et al., 2006; Arthur and Sageman, 2013). Organic-rich sediment formation is primarily driven by productivity. As such, total organic carbon (TOC), organic phosphorus, and organic barium contents are frequently used as proxies for ancient productivity (Schoepfer et al., 2015).

Phosphorus (P) is a key limiting nutrient in marine ecosystems (Paytan and McLaughlin, 2007). The concentration of P in the ocean is the ultimate limiting nutrient for primary production (Tyrell, 1999). A substantial amount of phosphorus is transported from the surface to submarine waters through the sinking of organic matter (Benitez-Nelson, 2000), which is the primary source of phosphorus in marine sediments. However, detrital phosphorus

typically constitutes less than 20% of total phosphorus (Schenau et al., 2005; Algeo and Ingall, 2007). In order to enhance the precision of our flux calculations for assessing biogenic phosphorus (P) fluxes, we opted to employ organic phosphorus (P_{org}) instead of total phosphorus (P or P_{tot}).

Barium (Ba) mainly originates from river discharge and accumulates in marine sediment as barite. Barite, employed as a paleoproductivity proxy, exhibits notable merits in terms of its refractory nature and remarkable burial efficiency, particularly under oxic conditions. It demonstrates a considerably higher sinking flux of barium (30-50%) compared to the sinking flux values of organic carbon and phosphorus (which remain below 10%) (Balakrishnan Nair et al., 2005; Paytan and Griffith, 2007). Barite is a stable mineral with a high burial efficiency (greater than 30%) and long residence time (Dymond et al., 1992), leading to localized Ba enrichment in sediment through the sinking of organic matter. This fraction is referred to as "biogenic Ba" (Babio). Despite the challenging conditions prevalent in reducing environments that are unfavorable for the preservation of barite, its efficacy as a paleoproductivity proxy remains significant due to the substantial influx of biogenic Ba to the sediment-water interface (Scopelliti et al., 2004; Bak, 2007). In this study, biogenic Ba is estimated

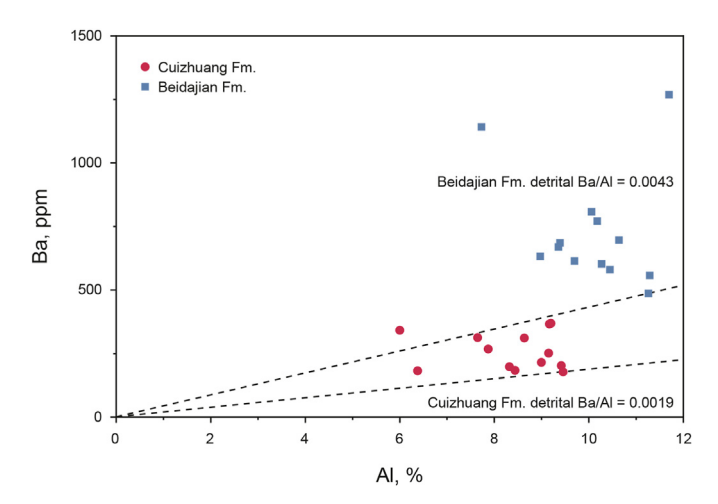


Fig. 4. Ba versus Al. The diagonal line represents the estimated detrital Ba fraction; additional Ba above this line represents the excess or biogenic Ba fraction.

using Eq. (3) to minimize potential errors from detrital Ba. The (Ba/Al)_{detr} ratios for the Cuizhuang Formation and Beidajian Formation are 0.0019 and 0.0043, respectively, based on Ba versus Al plots (Fig. 4).

This study analyzed the organic phosphorus (P_{org}) concentrations in the Cuizhuang and Beidajian Formations. The Cuizhuang Formation had P_{org} concentrations ranging from 24.12 to 572.69 ppm (average = 216.48 ppm), while the Beidajian Formation had concentrations ranging from 55.13 to 2969.27 ppm (average = 734.47 ppm). All are higher than the UCC (McLennan, 2001). The lower P_{org} concentration in the anoxic section of the Cuizhuang Formation may be due to the high efficiency of P cycling in the ocean, particularly under anoxic conditions (Benitez-Nelson, 2000), where P in sediments can rediffuse into the upper water column (Louchouarn et al., 1997). This phenomenon can lead to seawater eutrophication. Additionally, increased productivity can exacerbate oxygen depletion in seawater, which can further affect P concentrations. Thus, the low P concentration in the organic-rich section of the Cuizhuang Formation could be explained.

This study found that the Babio concentrations in the lower part of the Cuizhuang Formation ranged from 7 to 3306 ppm (average = 337 ppm), while the Babio values in the Beidajian Formation ranged from 2 to 809 ppm (average = 298 ppm), indicating moderate primary productivity (Algeo et al., 2011). The Babio concentration showed a clear increasing trend in the organic-rich interval of the lower part of the Cuizhuang Formation (Fig. 5). However, when using heavy minerals, such as barite, as proxies for paleoproductivity, it is important to consider that sulfate-reducing bacteria in suboxic or anoxic environments can reduce sulfates in barite, leading to the loss of biogenic Ba (McManus et al., 1998; Schoepfer et al., 2015). This may explain the relatively low Babio content in the lower part of the Cuizhuang Formation. The total organic carbon (TOC) content decreased from the lower part of the Cuizhuang Formation (0.093%-2.16%, average = 0.49%) to the Beidajian Formation (0.027%-0.215%, average = 0.13%). This decrease indicates that the highest level of productivity occurred during organic-rich sedimentation in the lower part of the Cuizhuang Formation.

5.3. Redox conditions

A qualitative assessment of ancient ocean redox conditions can be achieved through the enrichment of oxidation–reduction sensitive trace elements, including Mo_{EF} and C_{org}/P_{tot} ratios (Calvert

and Pedersen, 1993; Dean et al., 1997; Tribovillard et al., 2006). The Corg/Ptot ratio is significantly impacted by the oxidationreduction conditions of bottom water: reducing conditions lead to organic carbon preservation and phosphorus loss, while oxidizing conditions facilitate organic carbon degradation and phosphorus preservation (Algeo and Ingall, 2007; Kraal et al., 2012). The C-S-Fe-P proxies, specifically the C_{org}/P_{tot} ratio, provided more accurate results compared to the bimetal-ratio proxies, as indicated by previous research (Algeo and Liu, 2020). Previous research has suggested that Corg/Ptot ratios of <50, 50-200, and >200 correspond to oxic, suboxic, and anoxic conditions, respectively (Algeo and Ingall, 2007; Shen et al., 2015). Mo is present as molybdate (MoO_4^{2-}) in oxidizing environments, whereas in reducing environments, Mo(VI) is generally transformed into insoluble Mo(IV) (Kimura and Watanabe, 2001). Previous research has suggested that the most effective redox proxies are trace-metal EFs (Re, Ni, Mo) (Algeo and Liu, 2020). Hence, the degree of Mo enrichment can be utilized to reconstruct ancient redox conditions. Values of $Mo_{EF} > 1$ indicate anoxic conditions, whereas values of $Mo_{EF} < 1$ suggest oxic conditions (Algeo and Tribovillard, 2009).

The paleoredox indicators, C_{org}/P_{tot} and Mo_{EF} , exhibit similar trends (Fig. 5). Stratigraphically, both indicators show higher values in the organic-rich intervals of the lower part of the Cuizhuang Formation, which is consistent with the TOC content trends. On a longer timescale, ocean redox conditions have shifted from oxic in the Beidajian Formation to reducing in the lower part of the Cuizhuang Formation. Two black shale intervals in the lower part of the Cuizhuang Formation demonstrate anoxic conditions, which transition to suboxic conditions in the middle.

Mo and U exhibit different behaviors and enrichment mechanisms during sedimentary processes. In oxidizing seawater, U mainly exists as U(VI), but under suboxic conditions near the Fe(III) -Fe(II) transition, soluble U(VI) can be reduced to insoluble U(IV) and adsorbed onto Mn-hydroxides (Tribovillard et al., 2006). The transfer of U and Mo to sediments is facilitated by the presence of organic matter (Zheng et al., 2002; Tribovillard et al., 2006; Algeo and Tribovillard, 2009). Under these conditions, the precipitation rate of authigenic U is faster than that of authigenic Mo. As the sedimentary environment becomes more reducing and H2S is produced, molybdate (MoO₄²) is transformed into thiomolybdate $(MoO_{4-x}S_x^{2-})$ or molybdenum sulfides, which are captured by organic matter or iron sulfides (Zheng et al., 2000; Tribovillard et al., 2006; Helz et al., 2011). The trend of Mo self-enrichment is often greater than that of U under these conditions. Moreover, particle shuttling can accelerate the transfer of Mo to sediments, but U is not affected by this process (Crusius et al., 1996). Thus, the self-enrichment and covariation mechanisms of Mo-U in marine sediments serve as reliable indicators of changes in the redox conditions.

The Mo/U ratios in the Beidajian and lower Cuizhuang Formations follow an "unrestricted marine trend," with values approximately 0.3 times the seawater ratio, indicating deposition in a passive continental margin (Fig. 6). Beidajian Formation samples show U_{EF} values that are greater than Mo_{EF} values, showing sedimentary characteristics indicative of suboxic basins. With increasing anoxia, the data points move upward, indicating an increase in Mo_{EF} values, which is consistent with the sedimentary characteristics of the Cuizhuang Formation suboxic/anoxic basin. In open marine basins, the degree of Mo-U enrichment is positively correlated with the degree of anoxia (Zheng et al., 2000), as a low oxygen content favors the enrichment of redox-sensitive elements (RSMs), such as Mo and U. However, in restricted basins, the degree of Mo-U enrichment decreases with increasing anoxia, as the concentration of RSMs in sediment is primarily controlled by the RSM content in seawater rather than the bottom water redox

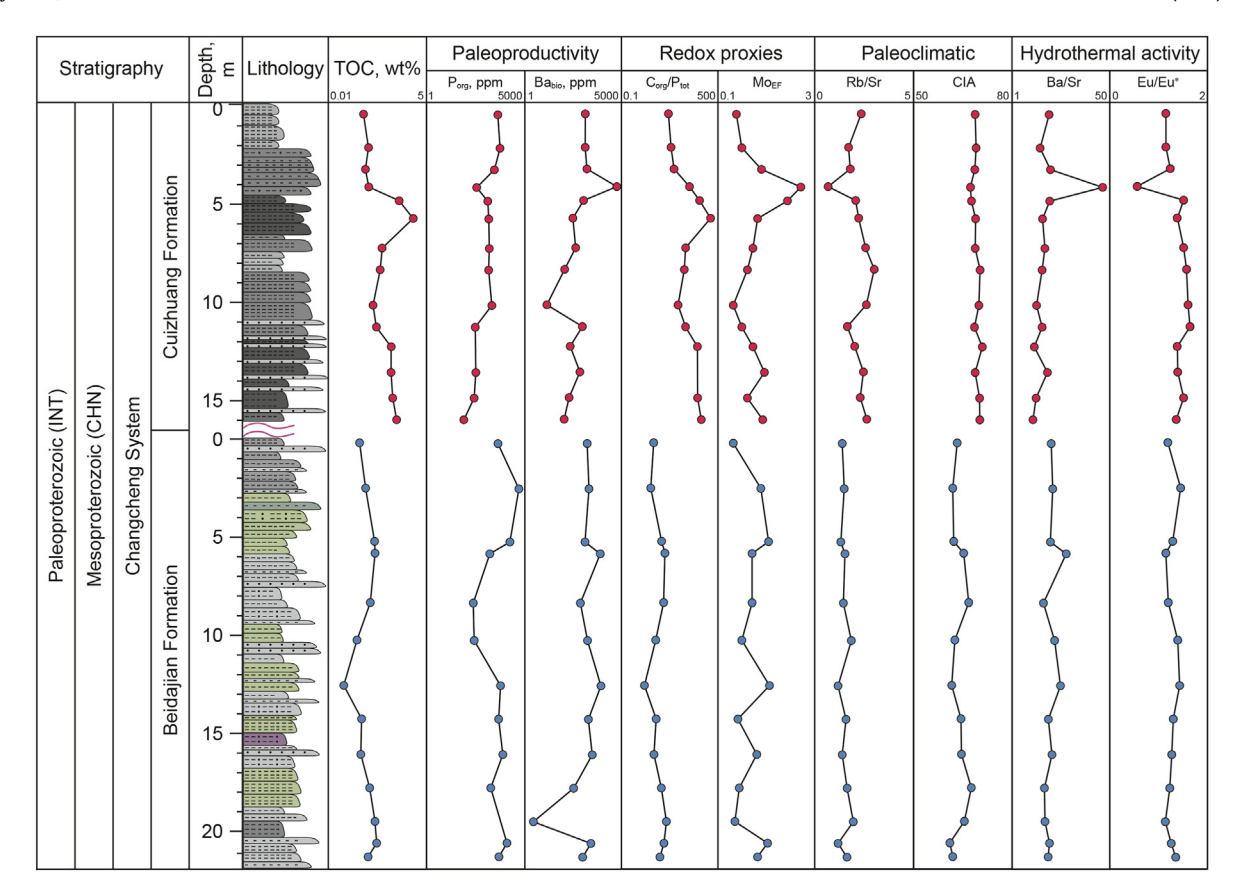


Fig. 5. Stratigraphic variation in TOC content, P, biogenic barium (Babio), Corg/Ptot ratio, molybdenum enrichment (MoEF), Rb/Sr ratio, CIA, Ba/Sr ratio and Eu/Eu* ratio.

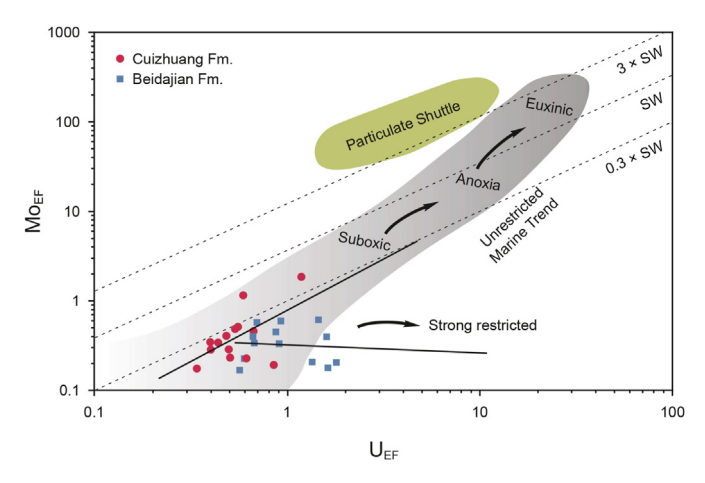


Fig. 6. Mo_{EF} versus U_{EF} in the Cuizhuang and Beidajian Formation. Solid lines show main covariant trends in each dataset, dotted lines show Mo/U molar ratios as multiples of the seawater value (3 \times SW, 1 \times SW, 0.3 \times SW).

conditions (Algeo and Lyons, 2006).

In summary, the redox proxies (Mo_{EF} , U_{EF} , and C_{org}/P_{tot}) indicate that the sedimentary environment from the Beidajian Formation to the lower Cuizhuang Formation experienced a cyclic change in redox conditions, with oxic-suboxic-anoxic-suboxic-anoxic transitions, which were possibly influenced by short-term sea-level changes (Haq and Schutter, 2008; Jin et al., 2020). This resulted in the formation of short-term cyclic redox patterns.

5.4. Relationship of TOC with marine productivity and redox conditions

Enhancing marine productivity and improving bottom water redox conditions are crucial for the preservation and accumulation of total organic carbon (TOC) in marine source rocks (Wei et al., 2012). In the Cuizhuang Formation, TOC is positively correlated with the redox proxies, $C_{\rm org}/P_{\rm tot}$ and $Mo_{\rm EF}$ (Fig. 7(c) and (d)), but seems not with P and Babio (Fig. 7(a) and (b)), indicating the significant role of redox conditions in controlling the organic matter accumulation in the Cuizhuang Formation shale. The impact of paleoproductivity on the deposition of organic-rich shale in the Cuizhuang Formation, however, is limited (Pan et al., 2020).

However, phosphorus (P) plays a crucial role in controlling primary production in the oceans and may also contribute to the regulation of atmospheric oxygen levels over geological time through various feedback mechanisms (Reinhard et al., 2017). When atmospheric oxygen concentrations are low, there is an expansion of anoxic (euxinic) environments, leading to increased sediment deposition with high C_{org}/P_{tot} ratios (Canfield et al., 2020). This results in a higher amount of organic carbon being buried relative to phosphorus, enabling greater organic carbon burial with a given phosphorus input to the oceans.

5.5. Mechanisms of organic matter enrichment

5.5.1. Paleoclimatic conditions

Paleomagnetic data show that the North China Plate was located in a tropical-subtropical climate zone during the Proterozoic era (Zhao et al., 1996; Halls et al., 2000). The Rb/Sr ratio is an effective

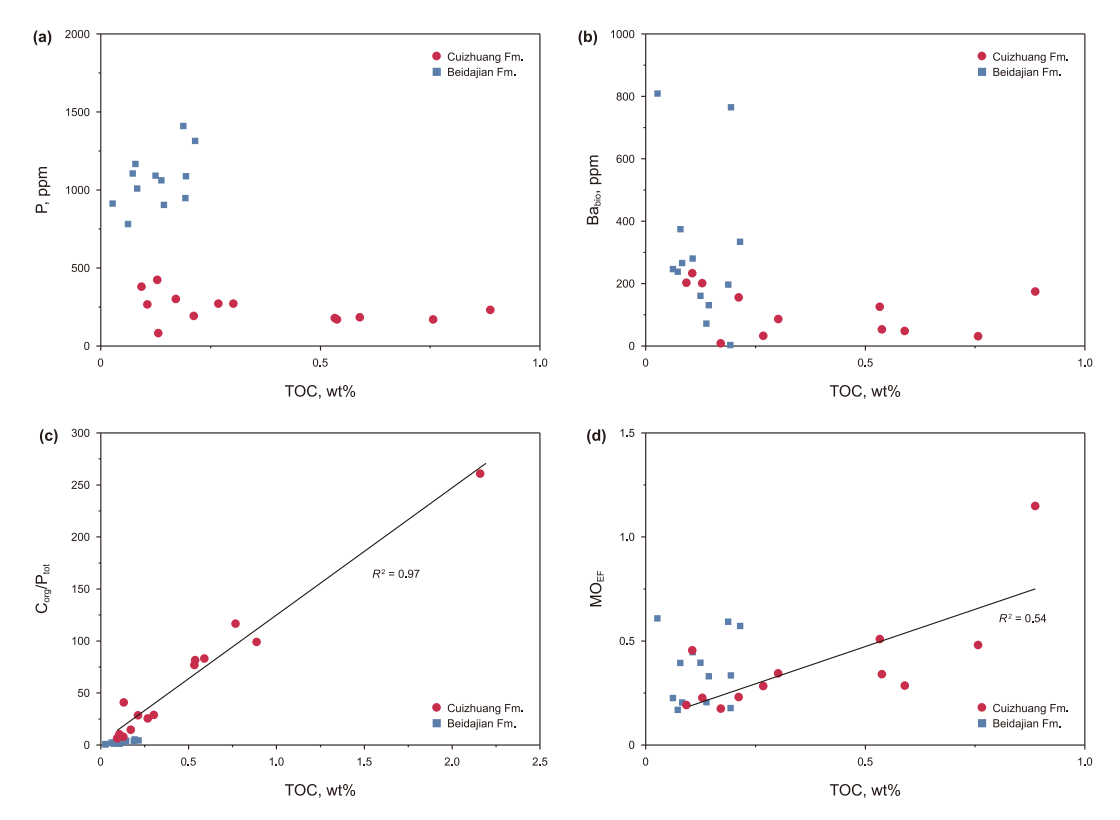


Fig. 7. (a) No relationship between biogenic barium (Ba_{bio}) and TOC contents. (b) No relationship between Phosphorus (P) and TOC contents. (c, d) Strong and moderate positive correlations between C_{org}/P_{tot} , U_{EF} , and TOC contents.

paleoclimate proxy, revealing characteristics such as temperature, humidity, and the chemical weathering degree (Chang et al., 2013; Liu et al., 2014; Hosek et al., 2015; Armstrong-Altrin and Machain-Castillo, 2016). A higher Rb/Sr ratio usually indicates a warm and humid climate and intense chemical weathering (Chang et al., 2013; Liu et al., 2014). For the sediments of the Cuizhuang and Beidajian Formations, their Rb/Sr ratios are higher than the PAAS ratio, indicating a warm and humid climate. The Cuizhuang Formation depositional environment had a stronger weathering intensity and a warmer and more humid climate than that of the Beidajian Formation, indicated by its higher Rb/Sr ratios.

The CIA is a widely used paleo-weathering index for evaluating the extent of chemical weathering in source areas (Nesbitt and Young, 1982). Generally, high CIA values (80–100) indicate hot and humid climates with intense chemical weathering, moderate values (60–80) suggest warm and humid conditions with moderate chemical weathering, and low values (50–60) indicate cold and arid climates with weak chemical weathering (Fedo et al., 1995). The average CIA values show a gradual increase from 63.88 (range 61.22–67.64) in the Beidajian Formation to 69.15 (range 67.36–70.93) in the lower Cuizhuang Formation shales. These findings indicate a rapid climate warming and intensified chemical weathering in the southern margin of the Ordos Basin of NCC, and this may be closely related to the vigorous late-stage rift tectonic activity.

5.5.2. Evidence for submarine hydrothermal activity

The concentration and distribution patterns of REEs in sedimentary rocks are important indicators of the source of mineral deposits and the nature of sedimentation, including the redox environment (Uysal et al., 2007; Censi et al., 2010; Kim et al., 2012; Shen et al., 2012; Zhu et al., 2014; Chen et al., 2015). Positive Eu anomalies are typically associated with hydrothermal activity (Kim

et al., 2012; Chen et al., 2015), while sediment influenced by hydrothermal activity can be identified by a depletion of LREE values and enrichment of HREE, unlike normal marine sediments which are typically characterized by LREE enrichment (Bau and Dulski, 1996; Parsapoor et al., 2009; Prakash et al., 2012; Chen et al., 2015). In our study, we found that samples from the Cuizhuang Formation displayed positive Eu anomalies (average Eu/Eu* values of 1.42). The PAAS-normalized REE patterns of the Cuizhuang Formation samples showed LREE depletion and HREE enrichment (mean $Nd_N/Yb_N = 0.93$; Fig. 8, Table 3), indicating that the sedimentation of the Cuizhuang shale was related to submarine hydrothermal activity.

REEs in mineral sources exhibit low and uniform Y/Ho ratios,

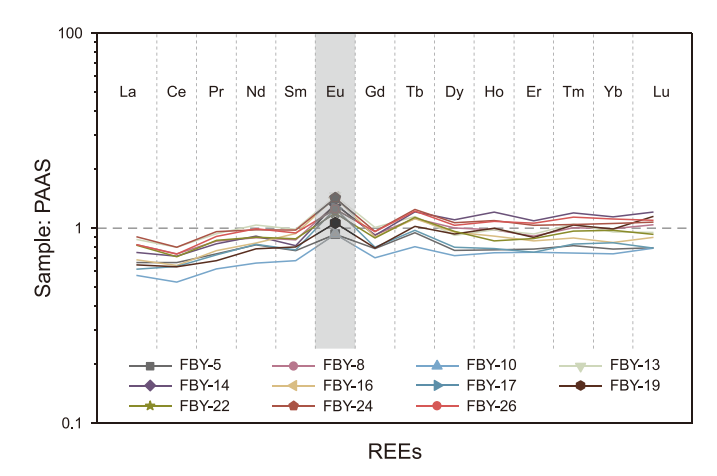


Fig. 8. PAAS-normalized REE distributions in sediments from the Cuizhuang Formation. The REE values in PAAS are from Pourmand et al. (2012).

with chondrites and igneous rocks typically displaying ratios of 26–28 (Nozaki et al., 1997; Zhai et al., 2000; Kamber and Webb, 2001). In contrast, seawater has higher and more variable Y/Ho ratio, usually 60–70 (Webb and Kamber, 2000; McLennan, 2001). Our study found that the Y/Ho ratios of samples from the lower part of the Cuizhuang Formation ranged from 23.5 to 28.0 (average of 25.5), indicating a closer similarity to chondrites than to seawater. This result suggests that the REEs in the rock samples from the lower part of the Cuizhuang Formation mainly originated from a mineral source, indicating a restricted basin environment during formation.

The Ba/Sr ratio is a useful indicator of submarine hydrothermal activity. Typically, Ba/Sr ratios are less than 1 in normal marine sedimentary rocks, but greater than 1 in hydrothermal sediment, with higher ratios indicating stronger hydrothermal activity (Peter and Scott, 1988; Kinman and Neal, 2006). In our study, samples from the lower part of the Cuizhuang Formation showed Ba/Sr ratios ranging from 2.31 to 37.64 (mean = 5.88). Due to barium loss during genesis, the original Ba/Sr ratio may be even higher than the measured value, indicating intense submarine hydrothermal activity during the sedimentation of the lower part of the Cuizhuang Formation.

5.5.3. Main factors controlling organic matter enrichment

The organic-rich interval in the lower part of the Cuizhuang Formation is likely influenced by multiple factors, including a warm-humid climate, submarine hydrothermal activity, and suboxic-anoxic conditions (Fig. 9). The warm-humid climate promoted chemical weathering that released nutrients and enhanced marine productivity (Deng et al., 2006; Hartmann et al., 2013). The relative sea-level rise caused by the warmer and more humid climate favored the development of suboxic-anoxic conditions. Hydrothermal activity provided additional nutrients and elements, such as P, Fe, Ni, and V (Varnavas and Cronan, 2005). Many studies have shown that productivity is correlated with the amount of hydrothermal input into the environment (Haymon et al., 1993; Geoffrey, 1998; Summit and Baross, 2001; Rusch et al., 2005). An increase in nutrient flux and productivity would lead to the consumption of bottom water oxygen, resulting in bottom water anoxia (Schwark and Frimmel, 2004; Van Bentum et al., 2012; Lash and Blood, 2014). Therefore, input from hydrothermal fluids from submarine waters may have contributed to the establishment of suboxic-anoxic bottom water conditions (Fig. 9). However, the warm-humid climate and submarine hydrothermal activity

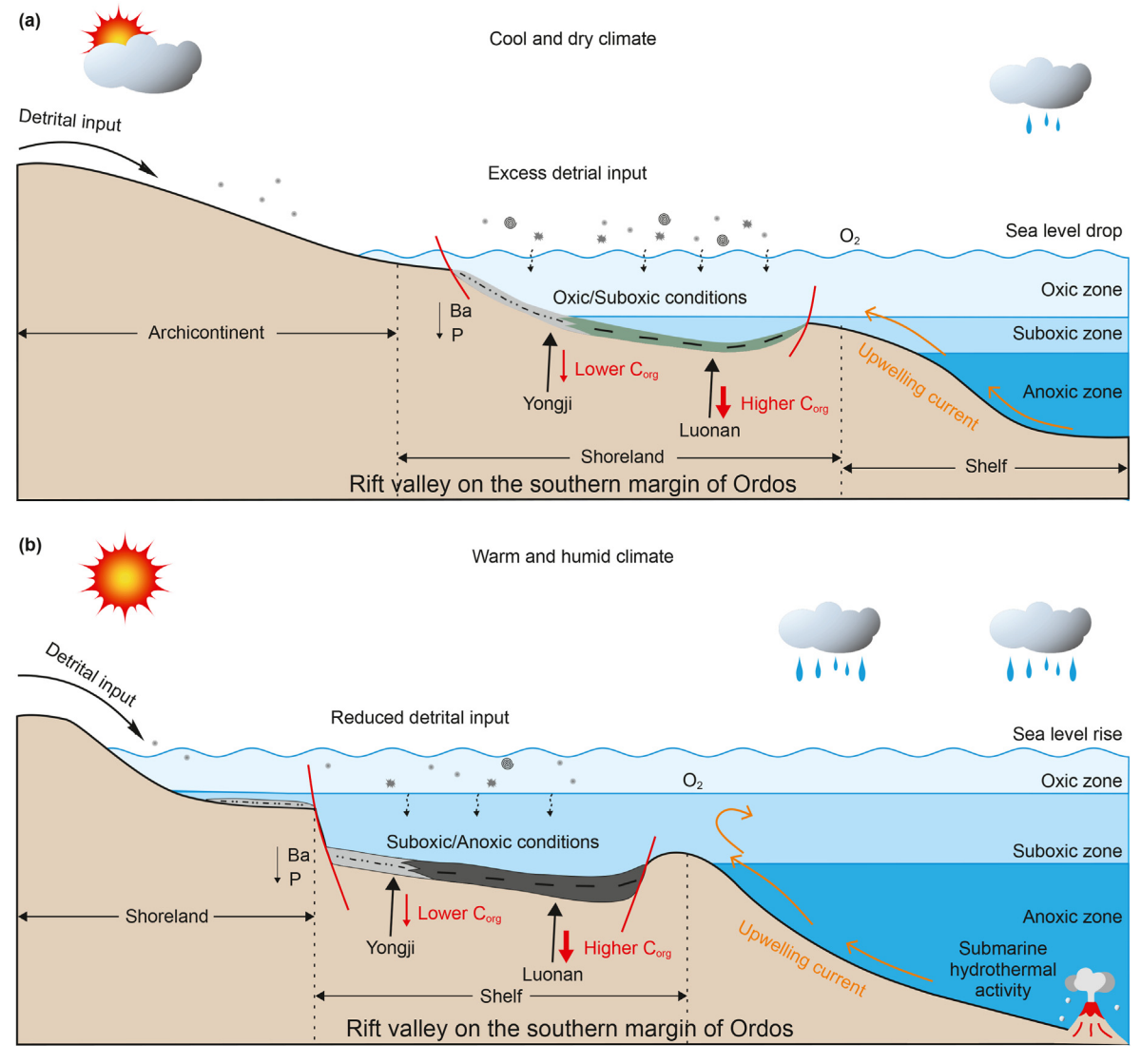


Fig. 9. Schematic diagram of organic matter enrichment models for the deposition of organic-rich Beidajian Fm. (a) and Cuizhuang Fm. (b) during Mesoproterozoic in North China.

indirectly influenced the redox environment, which was the main factor controlling organic matter enrichment in the lower part of the Cuizhuang Formation compared to the Beidajian Formation. Additionally, the Mo—U plot shows that the basin became more restricted, causing water residence that led to the depletion of redox-sensitive elements in the water column, which affected the redox environment. The relatively low concentrations of P and biogenic Ba in the Cuizhuang Formation indicate overall lower paleoproductivity, which may have greatly limited organic matter formation, resulting in a generally low TOC content.

Therefore, the deposition of organic-rich shales in the lower part of the Cuizhuang Formation is primarily controlled by suboxic to anoxic conditions, with submarine hydrothermal activity and climate having indirect effects. In contrast, the Beidajian Formation has a lower organic matter content and exhibits gray-green coloration due to the absence of submarine hydrothermal activity and a cold-dry climate, which resulted in euxinic bottom water conditions.

6. Conclusions

Based on the mineral composition analysis, the lithofacies of the lower Cuizhuang Formation and Beidajian Formation are classified into four layers: siliceous shale (S), argillaceous-rich siliceous shale (AS), argillaceous/siliceous mixed shale (ASM), and siliceous-rich argillaceous shale (SA). The Cuizhuang Formation was deposited in a relatively restricted sedimentary basin during the Mesoproterozoic rift stage. Compared to the Beidajian Formation, the Cuizhuang Formation experienced greater confinement due to tectonic movements, leading to enhanced water residence time and decreased supply of nutrients and redox-sensitive elements. This may have been a significant factor contributing to the lower overall total organic carbon (TOC) content in the lower Cuizhuang Formation. The deposition of organic-rich black shale in the lower Cuizhuang Formation corresponds to an increase in anoxic conditions. The influx of organic matter into submarine waters consumes dissolved oxygen in the water, establishing suboxic-anoxic bottom water conditions in the lower Cuizhuang Formation. The establishment of suboxic-anoxic conditions may significantly enhance the preservation efficiency of organic matter. Changes in anoxia are closely linked to a relatively warm and humid climate and submarine hydrothermal activity.

In summary, the coupled mechanism of a suboxic-reducing water environment, warm and humid climate, and submarine hydrothermal activity controlleds the development of hydrocarbon source rocks in the Mesoproterozoic Cuizhuang Formation.

Declaration of interest statement

No conflict of financial interest exits in the submission of this manuscript, and manuscript is approved by all authors for publication. I would like to declare on behalf of my co-authors that the work described was original research that has not been published previously, and not under consideration for publication elsewhere, in whole or in part.

CRediT authorship contribution statement

Zhi-Chen Wu: Writing — original draft, Methodology, Investigation, Formal analysis, Data curation, Conceptualization. **Ju-Ye Shi:** Writing — review & editing, Validation, Supervision, Methodology. **Tai-Liang Fan:** Writing — review & editing, Validation, Supervision, Funding acquisition. **Ming Jiang:** Methodology, Data curation.

Acknowledgments

This work is supported by the National Natural Science Foundation of China (Grant U19B6003-01-02, 42102150, 42372163).

References

- Algeo, T.J., Lyons, T.W., 2006. Mo-total organic carbon covariation in modern anoxic marine environments: implications for analysis of paleoredox and paleohydrographic conditions. Paleoceanography 21, PA1016. https://doi.org/10.1029/ 2004PA001112.
- Algeo, T.J., Ingall, E., 2007. Sedimentary Corg: P ratios, paleocean ventilation, and Phanerozoic atmospheric pO2. Paleogeogr. Paleoclimatol. Paleoecol. 256, 130–155. https://doi.org/10.1016/j.palaeo.2007.02.029.
- Algeo, T.J., Tribovillard, N., 2009. Environmental analysis of paleoceanographic systems based on molybdenum-uranium covariation. Chem. Geol. 268, 211–225. https://doi.org/10.1016/j.chemgeo.2009.09.001.
- Algeo, T.J., Kuwahara, K., Sano, H., Bates, S., Lyons, T., Elswick, E., Hinnov, L., Ellwood, B., Moser, J., Maynard, J.B., 2011. Spatial variation in sediment fluxes, redox conditions, and productivity in the Permian—Triassic Panthalassic Ocean. Paleogeogr. Paleoclimatol. Paleoecol. 308, 65–83. https://doi.org/10.1016/j.palaeo.2010.07.007.
- Algeo, T.J., Rowe, H., 2012. Paleoceanographic applications of trace-metal concentration data. Chem. Geol. 324, 6–18. https://doi.org/10.1016/j.chemgeo.2011.09.002.
- Algeo, T.J., Liu, J., 2020. A re-assessment of elemental proxies for paleoredox analysis. Chem. Geol. 540, 119549. https://doi.org/10.1016/j.chemgeo.2020.119549.
- Armstrong-Altrin, J.S., Machain-Castillo, M.L., 2016. Mineralogy, geochemistry, and radiocarbon ages of deep sea sediments from the Gulf of Mexico, Mexico. J. South Am. Earth Sci. 71, 182–200. https://doi.org/10.1016/j.jsames.2016.07.010.
- Arthur, M.A., Sageman, B.B., 2013. Sea-Level Control on Source-Rock Development: Perspectives from the Holocene Black Sea, the Mid-cretaceous Western Interior Basin of North America, and the Late Devonian Appalachian Basin. SEPM Special Publications, pp. 35–59. https://doi.org/10.2110/pec.05.82.0035.
- Bak, K., 2007. Organic-rich and manganese sedimentation during the Cenomanian—Turonian boundary event in the Outer Carpathian basins: a new record from the Skole Nappe, Poland. Paleogeogr. Paleoclimatol. Paleoecol. 256, 21–46. https://doi.org/10.1016/j.palaeo.2007.09.001.
- Balakrishnan Nair, T.M., Ittekkot, V., Shankar, R., Guptha, M.V.S., 2005. Settling barium fluxes in the Arabian Sea: critical evaluation of relationship with export production. Deep-Sea Res. Part II Top. Stud. Oceanogr. 52, 1930–1946. https:// doi.org/10.1016/j.dsr2.2005.06.003.
- Bau, M., Dulski, P., 1996. Distribution of yttrium and rare-earth elements in the penge and kuruman iron-formations, transvaal supergroup, South Africa. Precambrian Res. 79, 37–55. https://doi.org/10.1016/0301-9268(95)00087-9.
- Bazhenova, O.K., Arefev, O.A., Sokolov, B.A., 1994. Genetic features of Upper-Proterozoic oils. Doklady Akademii Nauk 337, 371—375.
- Bechtel, A., Jia, J.L., Strobl, S.A.I., Sachsenhofer, R.F., Liu, Z.J., Gratzer, R., Puttmann, W., 2012. Palaeoenvironmental conditions during deposition of the Upper Cretaceous oil shale sequences in the Songliao Basin (NE China): implications from geochemical analysis. Org. Geochem. 46, 76–95. https://doi.org/10.1016/j.orggeochem.2012.02.003.
- Benitez-Nelson, C.R., 2000. The biogeochemical cycling of phosphorus in marine systems. Earth Sci. Rev. 51, 109–135. https://doi.org/10.1016/S0012-8252(00) 00018-0
- Calvert, S.E., Pedersen, T.F., 1993. Geochemistry of recent oxic and anoxic marine-sediments implications for the geological record. Mar. Geol. 113, 67–88. https://doi.org/10.1016/0025-3227(93)90150-T.
- Canfield, D.E., Bjerrum, C.J., Zhang, S.C., Wang, H.J., Wang, X.M., 2020. The modern phosphorus cycle informs interpretations of Mesoproterozoic Era phosphorus dynamics. Earth Sci. Rev. 208, 103267. https://doi.org/10.1016/ i.earscirey.2020.103267.
- Censi, P., Incarbona, A., Oliveri, E., Bonomo, S., Tranchida, G., 2010. Yttrium and REE signature recognized in central mediterranean sea (ODP site 963) during the MIS 6–MIS 5 transition. Paleogeogr. Paleoclimatol. Paleoecol. 292, 201–210. https://doi.org/10.1016/i.palaeo.2010.03.045.
- Chang, H., An, Z.S., Wu, F., Jin, Z.D., Liu, W.G., Song, Y.G., 2013. A Rb/Sr record of the weathering response to environmental changes in westerly winds across the Tarim Basin in the late Miocene to the early Pleistocene. Paleogeogr. Paleoclimatol. Paleoecol. 386, 364–373. https://doi.org/10.1016/j.palaeo.2013.06.006.
- Chen, J.B., Algeo, T.J., Zhao, L.S., Chen, Z.Q., Cao, L., Zhang, L., Li, Y., 2015. Diagenetic uptake of rare earth elements by bioapatite, with an example from Lower Triassic conodonts of South China. Earth Sci. Rev. 149, 181–202. https://doi.org/ 10.1016/j.earscirev.2015.01.013.
- Chen, Y.Z., Fu, J.H., Yang, G.Y., Xiao, A.C., Sun, L.Y., Xu, B., Bao, H.P., Mao, L.G., 2016. Researches on basin property of Ordos block during mesoproterozoic Changcheng period. Acta Petrol. Sin. 32, 856–864.
- Crusius, J., Calvert, S., Pedersen, T., Sage, D., 1996. Rhenium and molybdenum enrichments in sediments as indicators of oxic, suboxic and sulfidic conditions of deposition. Earth Planet Sci. Lett. 145, 65–78. https://doi.org/10.1016/S0012-821X(96)00204-X.
- Dean, W.E., Gardner, J.V., Piper, D.Z., 1997. Inorganic geochemical indicators of

glacial-interglacial changes in productivity and anoxia on the California continental margin. Geochem. Cosmochim. Acta 61, 4507–4518. https://doi.org/10.1016/S0016-7037/9700237-8

- Deng, C.L., Shaw, J., Liu, Q.S., Pan, Y.X., Zhu, R.X., 2006. Mineral magnetic variation of the Jingbian loess/paleosol sequence in the northern Loess Plateau of China: implications for Quaternary development of Asian aridification and cooling. Earth Planet Sci. Lett. 241, 248–259. https://doi.org/10.1016/j.epsl.2005.10.020.
- Deng, Y., Wang, H.J., Lyu, D., Zhang, F.L., Gao, Z.Y., Ren, R., Ye, Y.T., Lyu, Y.T., Wang, X.M., Guan, P., Zhang, S.C., 2021. Evolution of the 1.8—1.6 Ga Yanliao and xiong'er basins, north China craton. Precambrian Res. 365, 106383. https://doi.org/10.1016/j.precamres.2021.106383.
- Dickas, A.B., 1986. Precambrian as a hydrocarbon exploration target. Geosci. Wis. 11, 5–7.
- Dong, T., Harris, N.B., Ayranci, K., 2017. Relative sea-level cycles and organic matter accumulation in shales of the Middle and Upper Devonian Horn River Group, northeastern British Columbia, Canada: insights into sediment flux, redox conditions, and bioproductivity. GSA Bulletin 130, 859–880. https://doi.org/ 10.1130/B31851.1.
- Dymond, J., Suess, E., Lyle, M., 1992. Barium in deep-sea sediment: a geochemical proxy for paleoproductivity. Paleoceanography 7, 163–181. https://doi.org/10.1029/92PA01080.
- Fedo, C.M., Nesbitt, H.W., Young, G.M., 1995. Unraveling the effects of potassium metasomatism in sedimentary-rocks and paleosols, with implications for paleoweathering conditions and provenance. Geology 23, 921–924. https://doi.org/10.1130/0091-7613(1995)023<0921:UTEOPM>2.3.CO, 2.
- Feng, Q.H., Xu, S.Q., Xing, X.D., Zhang, W., Wang, S., 2020. Advances and challenges in shale oil development: a critical review. Advances in Geo-Energy Research 4 (4), 406–418. https://doi.org/10.46690/ager.2020.04.06.
- Fowler, M.G., Douglas, A.G., 1987. Saturated- hydrocarbon biomarkers in oils of late precambrian age from eastern Siberia. Org. Geochem. 11, 201–213. https:// doi.org/10.1016/0146-6380(87)90023-4.
- Galushkin, Y.I., Yakovlev, G.E., Kuprin, V.F., 2004. Catagenesis of Riphean and Vendian deposits in western Bashkortostan and realization of the hydrocarbon potential of their organic matter: numerical estimates. Geochem. Int. 42, 67–76.
- Geoffrey, P.G., 1998. Earliest life in the Archean: rapid dispersal of CO₂-utilizing bacteria from submarine hydrothermal vents. Episodes 21, 252–256. https://doi.org/10.18814/epiiugs/1998/v21i4/007.
- Goldberg, K., Humayun, M., 2010. The applicability of the chemical index of alteration as a paleoclimatic indicator: an example from the permian of the parana basin. Brazil. Paleogeogr. Paleoclimatol. Paleoecol. 293, 175–183. https://doi.org/10.1016/j.palaeo.2010.05.015.
- Goodarzi, F., Goodarzi, N.N., Malachowska, A., 2021. Elemental composition, environment of deposition of the lower Carboniferous Emma Fiord formation oil shale in Arctic Canada. Int. J. Coal Geol. 244. https://doi.org/10.1016/i.coal.2021.103715.
- Halls, H.C., Li, J.H., Davis, D., Hou, G., Zhang, B.X., Qian, X.L., 2000. A precisely dated Proterozoic palaeomagnetic pole from the North China craton, and its relevance to palaeocontinental reconstruction. Geophys. J. Int. 143, 185–203. https:// doi.org/10.1046/j.1365-246x.2000.00231.x.
- Hao, S.L., Sun, L.Y., Bao, H.P., Liu, G., Zhang, G.S., 2016. Exploration direction and potential of the middle-upper proterozoic in Ordos Basin. Nat. Gas Geosci. 27, 2127–2135. https://doi.org/10.11764/j.issn.1672-1926.2016.12.2127 (in Chinese).
- Haq, B.U., Schutter, S.R., 2008. A chronology of Paleozoic sea-level changes. Science 322, 64–68. https://doi.org/10.1126/science.1161648.
- Hartmann, J., West, A.J., Renforth, P., Köhler, P., De La Rocha, C.L., Wolf-Gladrow, D.A., Dürr, H.H., Scheffran, J., 2013. Enhanced chemical weathering as a geoengineering strategy to reduce atmospheric carbon dioxide, supply nutrients, and mitigate ocean acidification. Rev. Geophys. 51, 113–149. https://doi.org/ 10.1002/rog.20004.
- Haymon, R.M., Fornari, D.J., Von Damm, K.L., Lilley, M.D., Perfit, M.R., Edmond, J.M., Shanks, W.C., Lutz, R.A., Grebmeier, J.M., Carbotte, S., Wright, D., McLaughlin, E., Smith, M., Beedle, N., Olson, E., 1993. Volcanic eruption of the mid-ocean ridge along the East Pacific Rise crest at 9°45–52′N: direct submersible observations of seafloor phenomena associated with an eruption event in April, 1991. Earth Planet Sci. Lett. 119, 85–101. https://doi.org/10.1016/0012-821X(93)90008-W.
- He, Q., Dong, T., He, S., Zhai, G.Y., Guo, X.W., Hou, Y.G., Yang, R., Han, Y.J., 2020. Sedimentological and geochemical characterization of the Upper Permian transitional facies of the Longtan Formation, northern Guizhou Province, southwest China: insights into paleo-environmental conditions and organic matter accumulation mechanisms. Mar. Petrol. Geol. 118, 104446. https://doi.org/10.1016/j.marpetgeo.2020.104446.
- Helz, G.R., Bura-Nakic, E., Mikac, N., Ciglenecki, I., 2011. New model for molybdenum behavior in euxinic waters. Chem. Geol. 284, 323–332. https://doi.org/10.1016/ i.chemgeo.2011.03.012.
- Hosek, J., Hambach, U., Lisa, L., Grygar, T.M., Horacek, I., Meszner, S., Knesl, I., 2015. An integrated rock-magnetic and geochemical approach to loess/paleosol sequences from Bohemia and Moravia (Czech Republic): implications for the Upper Pleistocene paleoenvironment in central Europe. Paleogeogr. Paleoclimatol. Paleoecol. 418, 344–358. https://doi.org/10.1016/j.palaeo.2014.11.024.
- Jin, C.S., Liao, Z.W., Tang, Y.J., 2020. Sea-level changes control organic matter accumulation in the Longmaxi shales of southeastern Chongqing, China. Mar. Petrol. Geol. 119, 104478. https://doi.org/10.1016/j.marpetgeo.2020.104478.
- Jin, Z.J., 2023. Hydrocarbon accumulation and resources evaluation: recent advances and current challenges. Advances in Geo-Energy Research 8 (1), 1–4. https://doi.org/10.46690/ager.2023.04.01.

Kamber, B.S., Webb, G.E., 2001. The geochemistry of late Archaean microbial carbonate: implications for ocean chemistry and continental erosion history. Geochem. Cosmochim. Acta 65, 2509–2525. https://doi.org/10.1016/S0016-7037(01)00613-5.

- Khaled, A., Li, R.X., Xi, S.L., Zhao, B.S., Wu, X.L., Yu, Q., Zhang, Y.N., Li, D.L., 2022. Paleoenvironmental conditions and organic matter enrichment of the late paleoproterozoic Cuizhuang Formation dark shale in the Yuncheng Basin, north China. J. Pet. Sci. Eng. 208, 109627. https://doi.org/10.1016/j.petrol.2021.109627.
- Kim, J.-H., Torres, M.E., Haley, B.A., Kastner, M., Pohlman, J.W., Riedel, M., Lee, Y.-J., 2012. The effect of diagenesis and fluid migration on rare earth element distribution in pore fluids of the northern Cascadia accretionary margin. Chem. Geol. 291, 152–165. https://doi.org/10.1016/j.chemgeo.2011.10.010.
- Kimura, H., Watanabe, Y., 2001. Oceanic anoxia at the Precambrian-Cambrian boundary. Geology 29, 995–998. https://doi.org/10.1130/0091-7613(2001) 029<0995:OAATPC>2.0.CO, 2.
- Kinman, W.S., Neal, C.R., 2006. Magma evolution revealed by anorthite-rich plagioclase cumulate xenoliths from the Ontong Java Plateau: insights into LIP magma dynamics and melt evolution. J. Volcanol. Geoth. Res. 154, 131–157. https://doi.org/10.1016/j.jvolgeores.2005.09.024.
- Kraal, P., Slomp, C.P., Reed, D.C., Reichart, G.J., Poulton, S.W., 2012. Sedimentary phosphorus and iron cycling in and below the oxygen minimum zone of the northern Arabian Sea. Biogeosciences 9, 2603–2624. https://doi.org/10.5194/ bg-9-2603-2012.
- Kuznetsov, V.G., 1997. Riphean hydrocarbon reservoirs of the yurubchen-tokhom zone, lena-tunguska Province, NE Russia. J. Petrol. Geol. 20, 459–474. https:// doi.org/10.1111/i.1747-5457.1997.tb00926.x.
- Lash, G.G., Blood, D.R., 2014. Organic matter accumulation, redox, and diagenetic history of the Marcellus Formation, southwestern Pennsylvania, Appalachian basin. Mar. Petrol. Geol. 57, 244–263. https://doi.org/10.1016/ j.marpetgeo.2014.06.001.
- Li, Z.H., Xi, S.L., Hu, J.M., Dong, X.P., Zhang, G.S., 2019. New insights about the mesoproterozoic sedimentary framework of North China craton. Geol. J. 54, 409–425. https://doi.org/10.1002/gj.3190.
- Liu, B., Jin, H.L., Sun, L.Y., Sun, Z., Niu, Q.H., Xie, S.B., Li, G.H., 2014. Holocene moisture change revealed by the Rb/Sr ratio of aeolian deposits in the southeastern Mu Us Desert, China. Aeolian Res 13, 109—119. https://doi.org/10.1016/j.aeolia.2014.03.006.
- Liu, Q.Y., Zhu, D.Y., Jin, Z.J., Meng, Q.Q., Li, S.J., 2019. Influence of volcanic activities on redox chemistry changes linked to the enhancement of the ancient Sinian source rocks in the Yangtze craton. Precambrian Res. 327, 1–13. https://doi.org/ 10.1016/j.precamres.2019.02.017.
- Liu, Q.Y., Li, P., Jin, Z.J., Liang, X.P., Zhu, D.Y., Wu, X.Q., Meng, Q.Q., Liu, J.Y., Fu, Q., Zhao, J.H., 2021. Preservation of organic matter in shale linked to bacterial sulfate reduction (BSR) and volcanic activity under marine and lacustrine depositional environments. Mar. Petrol. Geol. 127, 104950. https://doi.org/10.1016/j.marpetgeo.2021.104950.
- Louchouarn, P., Lucotte, M., Duchemin, E., de Vernal, A., 1997. Early diagenetic processes in recent sediments of the Gulf of St-Lawrence: phosphorus, carbon and iron burial rates. Mar. Geol. 139, 181–200. https://doi.org/10.1016/S0025-3227(96)00110-7
- Luo, Q.Y., Zhong, N.N., Wang, Y.N., Zhang, Y.Q., Qin, J., Qi, L., Ma, Y., Zhang, Y., Zhu, S.L., Huang, X.Y., 2013. Geochemistry of mesoproterozoic hongshuizhuang formation shales in NorthernNorth China: implications for provenance and source weathering. Acta Geol. Sin. 87, 1913—1921. https://doi.org/10.19762/j.cnki.dizhixuebao.2013.12.013 (in Chinese).
- Lyu, D., Deng, Y., Wang, X.M., Ye, Y.T., Pang, K., Miao, L.Y., Luo, Z., Zhang, F.L., Lu, Y.Z., Deng, S.H., Wang, H.J., Zhang, S.C., 2022. New chronological and paleontological evidence for Paleoproterozoic eukaryote distribution and stratigraphic correlation between the Yanliao and Xiong'er basins, North China Craton. Precambrian Res. 371, 106577. https://doi.org/10.1016/j.precamres.2022.106577.
- McLennan, S.M., 2001. Relationships between the trace element composition of sedimentary rocks and upper continental crust. G-cubed 2. https://doi.org/10.1029/2000gc000109.
- McManus, J., Berelson, W.M., Klinkhammer, G.P., Johnson, K.S., Coale, K.H., Anderson, R.F., Kumar, N., Burdige, D.J., Hammond, D.E., Brumsack, H.J., McCorkle, D.C., Rushdi, A., 1998. Geochemistry of barium in marine sediments: implications for its use as a paleoproxy. Geochem. Cosmochim. Acta 62, 3453–3473. https://doi.org/10.1016/S0016-7037(98)00248-8.
- Meng, F.W., Zhou, C.M., Yin, L.M., Chen, Z.L., Yuan, X.L., 2005. The oldest known dinoflagellates: morphological and molecular evidence from Mesoproterozoic rocks at Yongji, Shanxi Province. Chin. Sci. Bull.-Chin. 50, 1230–1234. https:// doi.org/10.1360/982004-543 (in Chinese).
- Meng, Y., Zuo, P.F., Zheng, D.S., Sun, F.B., Wang, P.X., Wang, Z.J., Li, Y., 2018. The earliest clastic sediments overlying the Xiong'er volcanic rocks: implications for the Mesoproterozoic tectonics of the southern North China Craton. Precambrian Res. 305, 268–282. https://doi.org/10.1016/j.precamres.2017.12.001.
- Milliken, K.L., Esch, W.L., Reed, R.M., Zhang, T.W., 2012. Grain assemblages and strong diagenetic overprinting in siliceous mudrocks, barnett shale (mississippian), fort worth basin, Texas. AAPG (Am. Assoc. Pet. Geol.) Bull. 96, 1553–1578. https://doi.org/10.1306/12011111129.
- Murray, R.W., Leinen, M., 1993. Chemical transport to the seafloor of the equatorial Pacific Ocean across a latitudinal transect at 135°W: tracking sedimentary major, trace, and rare earth element fluxes at the Equator and the Intertropical Convergence Zone. Geochem. Cosmochim. Acta 57, 4141–4163. https://doi.org/10.1016/0016-7037(93)90312-K.

Nesbitt, H.W., Young, G.M., 1982. Early Proterozoic climates and plate motions inferred from major element chemistry of lutites. Nature 299, 715–717. https://doi.org/10.1038/299715-0

- Nozaki, Y., Zhang, J., Amakawa, H., 1997. The fractionation between Y and Ho in the marine environment. Earth Planet Sci. Lett. 148, 329–340. https://doi.org/10.1016/S0012-821X(97)00034-4.
- Pan, X., Wang, Z.L., Li, Q.Y., Gao, J., Zhu, L.W., Liu, W.H., 2020. Sedimentary environments and mechanism of organic matter enrichment of dark shales with low TOC in the Mesoproterozoic Cuizhuang Formation of the Ordos Basin: evidence from petrology, organic geochemistry, and major and trace elements. Mar. Petrol. Geol. 122, 104695. https://doi.org/10.1016/j.marpetgeo.2020.104695.
- Parsapoor, A., Khalili, M., Mackizadeh, M.A., 2009. The behaviour of trace and rare earth elements (REE) during hydrothermal alteration in the Rangan area (Central Iran). J. Asian Earth Sci. 34, 123–134. https://doi.org/10.1016/j.jseaes.2008.04.005.
- Paytan, A., Griffith, E.M., 2007. Marine barite: recorder of variations in ocean export productivity. Deep-Sea Res. Part II Top. Stud. Oceanogr. 54, 687–705. https:// doi.org/10.1016/j.dsr2.2007.01.007.
- Paytan, A., McLaughlin, K., 2007. The oceanic phosphorus cycle. Chem. Rev. 107, 563–576. https://doi.org/10.1021/cr0503613.
- Peter, J.M., Scott, S.D., 1988. Mineralogy, composition, and fluid-inclusion microthermometry of seafloor hydrothermal deposits in the Southern Trough of Guaymas Basin, Gulf of California. Can. Mineral. 26 (3), 567–587.
- Pourmand, A., Dauphas, N., Ireland, T.J., 2012. A novel extraction chromatography and MC-ICP-MS technique for rapid analysis of REE, Sc and Y: revising Cl-chondrite and Post-Archean Australian Shale (PAAS) abundances. Chem. Geol. 291, 38–54. https://doi.org/10.1016/j.chemgeo.2011.08.011.
- Prakash, L.S., Ray, D., Paropkari, A.L., Mudholkar, A.V., Satyanarayanan, M., Sreenivas, B., Chandrasekharam, D., Kota, D., Raju, K.A.K., Kaisary, S., Balaram, V., Gurav, T., 2012. Distribution of REEs and yttrium among major geochemical phases of marine Fe-Mn-oxides: comparative study between hydrogenous and hydrothermal deposits. Chem. Geol. 312, 127–137. https://doi.org/10.1016/i.chemseo.2012.03.024.
- Qiao, X.F., Wang, Y.B., 2014. Discussions on the lower boundary age of the mesoproterozoic and basin tectonic evolution of the mesoproterozoic in North China craton. Acta Geol. Sin. 88, 1623—1637. https://doi.org/10.19762/j.cnki.dizhixuebao.2014.09.001 (in Chinese).
- Qin, J., Zhong, N.N., Qi, W., Zhang, Y.Q., Luo, Q.Y., 2010. Organic petrology of the hongshuizhuang Formation in northern north China. Oil Gas Geol. 31, 367—374.
- Reinhard, C.T., Planavsky, N.J., Gill, B.C., Ozaki, K., Robbins, L.J., Lyons, T.W., Fischer, W.W., Wang, C., Cole, D.B., Konhauser, K.O., 2017. Evolution of the global phosphorus cycle. Nature 541, 386–389. https://doi.org/10.1038/nature20772.
- Rusch, A., Walpersdorf, E., DeBeer, D., Gurrieri, S., Amend, J.P., 2005. Microbial communities near the oxic/anoxic interface in the hydrothermal system of Vulcano Island. Italy. Chem. Geol. 224, 169–182. https://doi.org/10.1016/ j.chemgeo.2005.07.026.
- Schenau, S.J., Reichart, G.J., De Lange, G.J., 2005. Phosphorus burial as a function of paleoproductivity and redox conditions in Arabian Sea sediments. Geochem. Cosmochim. Acta 69, 919–931. https://doi.org/10.1016/j.gca.2004.05.044.
- Schoepfer, S.D., Shen, J., Wei, H.Y., Tyson, R.V., Ingall, E., Algeo, T.J., 2015. Total organic carbon, organic phosphorus, and biogenic barium fluxes as proxies for paleomarine productivity. Earth Sci. Rev. 149, 23–52. https://doi.org/10.1016/j.earscirev.2014.08.017.
- Schwark, L., Frimmel, A., 2004. Chemostratigraphy of the Posidonia Black Shale, SW-Germany: II. Assessment of extent and persistence of photic-zone anoxia using aryl isoprenoid distributions. Chem. Geol. 206, 231–248. https://doi.org/ 10.1016/j.chemgeo.2003.12.008.
- Scopelliti, G., Bellanca, A., Coccioni, R., Luciani, V., Neri, R., Baudin, F., Chiari, M., Marcucci, M., 2004. High-resolution geochemical and biotic records of the tethyan 'bonarelli level' (OAE2, latest cenomanian) from the calabianca–guidaloca composite section, northwestern sicily. Italy. Paleogeogr. Paleoclimatol. Paleoecol. 208, 293–317. https://doi.org/10.1016/j.palaeo.2004.03.012.
- Shen, J., Algeo, T.J., Hu, Q., Zhang, N., Zhou, L., Xia, W.C., Xie, S.C., Feng, Q.L., 2012. Negative C-isotope excursions at the Permian-Triassic boundary linked to volcanism. Geology 40, 963–966. https://doi.org/10.1130/G33329.1.
- Shen, J., Schoepfer, S.D., Feng, Q.L., Zhou, L., Yu, J.X., Song, H.Y., Wei, H.Y., Algeo, T.J., 2015. Marine productivity changes during the end-Permian crisis and Early Triassic recovery. Earth Sci. Rev. 149, 136–162. https://doi.org/10.1016/ j.earscirev.2014.11.002.
- Shi, X.Y., Zhang, C.H., Jiang, G.Q., Liu, J., Wang, Y., Liu, D.B., 2008. Microbial mats in the mesoproterozoic carbonates of the North China platform and their potential for hydrocarbon generation. J. China Univ. Geosci. 19, 549–566. https://doi.org/ 10.1016/S1002-0705(08)60060-6 (in Chinese).
- Song, Y., Li, S.F., Hu, S.Z., 2019. Warm-humid paleoclimate control of salinized lacustrine organic-rich shale deposition in the Oligocene Hetaoyuan Formation of the Biyang Depression, East China. Int. J. Coal Geol. 202, 69–84. https://doi.org/10.1016/j.coal.2018.11.016.
- Summit, M., Baross, J.A., 2001. A novel microbial habitat in the mid-ocean ridge subseafloor. Proc. Natl. Acad. Sci. U.S.A. 98, 2158–2163. https://doi.org/10.1073/ pnas.051516098.
- Taylor, S.R., Mclennan, S.M., 1985. The continental crust: its composition and evolution. An examination of the geochemical record preserved in sedimentary rocks. Science 231, 751–752. https://doi.org/10.1126/science.231.4739.751.

Thyberg, B., Jahren, J., 2011. Quartz cementation in mudstones: sheet-like quartz cement from clay mineral reactions during burial. Petrol. Geosci. 17, 53–63. https://doi.org/10.1144/1354-079310-028.

- Tribovillard, N., Algeo, T.J., Lyons, T., Riboulleau, A., 2006. Trace metals as paleoredox and paleoproductivity proxies: an update. Chem. Geol. 232, 12–32. https://doi.org/10.1016/j.chemgeo.2006.02.012.
- Tyrell, T., 1999. The relative influences of nitrogen and phosphorus on oceanic primary production. Nature 400 (6744), 525–531. https://doi.org/10.1038/22941
- Uysal, I.T., Zhao, J.X., Golding, S.D., Lawrence, M.G., Glikson, M., Collerson, K.D., 2007. Sm-Nd dating and rare-earth element tracing of calcite: implications for fluid-flow events in the Bowen Basin, Australia. Chem. Geol. 238, 63–71. https://doi.org/10.1016/j.chemgeo.2006.10.014.
- Van Bentum, E.C., Reichart, G.J., Damste, J.S.S., 2012. Organic matter provenance, palaeoproductivity and bottom water anoxia during the Cenomanian/Turonian oceanic anoxic event in the Newfoundland Basin (northern proto North Atlantic Ocean). Org. Geochem. 50, 11–18. https://doi.org/10.1016/j.orggeochem.2012.05.013.
- Varnavas, S.P., Cronan, D.S., 2005. Submarine hydrothermal activity off santorini and milos in the central hellenic volcanic arc: a synthesis. Chem. Geol. 224, 40–54. https://doi.org/10.1016/j.chemgeo.2005.07.013.
- Wang, J., Li, Z.X., 2003. History of Neoproterozoic rift basins in South China: implications for Rodinia break-up. Precambrian Res. 122, 141–158. https://doi.org/10.1016/S0301-9268(02)00209-7.
- Wang, K., Wang, T.S., Wang, Z.C., Luo, P., Li, Q.F., Fang, J., Ma, K., 2018. Characteristics and hydrocarbon geological conditions of the Changchengian rifts in the southern North China Craton. Acta Pet. Sin. 39, 504–517. https://doi.org/10.7623/syxb201805002 (in Chinese).
- Wang, P., Du, Y.S., Yu, W.C., Algeo, T.J., Zhou, Q., Xu, Y., Qi, L., Yuan, L.J., Pan, W., 2020a. The chemical index of alteration (CIA) as a proxy for climate change during glacial-interglacial transitions in Earth history. Earth Sci. Rev. 201, 103032. https://doi.org/10.1016/j.earscirev.2019.103032.
- Wang, T.G., Han, K.Y., 2011. On Meso-Neoproterozoic primary petroleum resources. Acta Pet. Sin. 32, 1—7.
- Wang, W.Y., Pang, X.Q., Wang, Y.P., Chen, Z.X., Li, C.R., Ma, X.H., 2022a. Hydrocarbon expulsion model and resource potential evaluation of high-maturity marine source rocks in deep basins: example from the Ediacaran microbial dolomite in the Sichuan Basin, China. Petrol. Sci. 19 (6), 2618—2630. https://doi.org/10.1016/j.petsci.2022.11.018.
- Wang, W.Y., Pang, X.Q., Chen, Z.X., Chen, D.X., Ma, X.H., Zhu, W.P., Zheng, T.Y., Wu, K.L., Zhang, K., Ma, K.Y., 2020b. Improved methods for determining effective sandstone reservoirs and evaluating hydrocarbon enrichment in petroliferous basins. Appl. Energy 261, 114457. https://doi.org/10.1016/j.apenergy.2019.114457.
- Wang, W.Y., Pang, X.Q., Chen, Z.X., Chen, D.X., Zheng, T.Y., Luo, B., Li, J., Yu, R., 2019. Quantitative prediction of oil and gas prospects of the sinian-lower paleozoic in the sichuan Basin in central China. Energy 174, 861–872. https://doi.org/ 10.1016/j.energy.2019.03.018.
- Wang, X.N., Li, J.R., Jiang, W.Q., Zhang, H., Feng, Y.L., Yang, Z., 2022b. Characteristics, current exploration practices, and prospects of continental shale oil in China. Advances in Geo-Energy Research 6 (6), 454–459. https://doi.org/10.46690/ager.2022.06.02.
- Webb, G.E., Kamber, B.S., 2000. Rare earth elements in Holocene reefal microbialites: a new shallow seawater proxy. Geochem. Cosmochim. Acta 64, 1557–1565. https://doi.org/10.1016/S0016-7037(99)00400-7.
- Wei, H.Y., Chen, D.Z., Wang, J.G., Yu, H., Tucker, M.E., 2012. Organic accumulation in the lower Chihsia Formation (Middle Permian) of South China: constraints from pyrite morphology and multiple geochemical proxies. Paleogeogr. Paleoclimatol. Paleoecol. 353–355, 73–86. https://doi.org/10.1016/ j.palaeo.2012.07.005.
- Xu, C., Shan, X.L., He, W.T., Zhang, K., Rexiti, Y., Su, S.Y., Liang, C., Zou, X.T., 2021. The influence of paleoclimate and a marine transgression event on organic matter accumulation in lacustrine black shales from the Late Cretaceous, southern Songliao Basin, Northeast China. Int. J. Coal Geol. 246. https://doi.org/10.1016/ j.coal.2021.103842.
- Xu, J.J., Liu, Z.J., Bechtel, A., Meng, Q.T., Sun, P.C., Jia, J.L., Cheng, L.J., Song, Y., 2015. Basin evolution and oil shale deposition during Upper Cretaceous in the Songliao Basin (NE China): implications from sequence stratigraphy and geochemistry. Int. J. Coal Geol. 149, 9–23. https://doi.org/10.1016/j.coal.2015.07.005.
- Zhai, M.G., 2013. The main old lands in China and assembly of Chinese unified continent. Sci. China Earth Sci. 56, 1829—1852. https://doi.org/10.1007/s11430-013-4665-7.
- Zhai, M.G., Bian, A.G., Zhao, T.P., 2000. The amalgamation of the supercontinent of North China Craton at the end of Neo-Archaean and its breakup during late Palaeoproterozoic and Meso-Proterozoic. Sci. China Earth Sci. 43, 219–232. https://doi.org/10.1007/BF02911947.
- Zhao, G.C., Cawood, P.A., Wilde, S.A., Sun, M., 2002. Review of global 2.1–1.8 Ga orogens: implications for a pre-Rodinia supercontinent. Earth Sci. Rev. 59, 125–162. https://doi.org/10.1016/S0012-8252(02)00073-9.
- Zhao, W.Z., Hu, S.Y., Wang, Z.C., Zhang, S.C., Wang, T.S., 2018. Petroleum geological conditions and exploration importance of Proterozoic to Cambrian in China. Petrol. Explor. Dev. 45, 1–14. https://doi.org/10.1016/S1876-3804(18)30001-6.
- Zhao, X., Coe, R.S., Gilder, S.A., Frost, G.M., 1996. Palaeomagnetic constraints on the palaeogeography of China: implications for gondwanaland. Aust. J. Earth Sci. 43,

- 643–672. https://doi.org/10.1080/08120099608728285.
 Zheng, Y., Anderson, R.F., Van Geen, A., Fleisher, M.Q., 2002. Remobilization of authigenic uranium in marine sediments by bioturbation. Geochem. Cosmochim. Acta 66, 1759-1772. https://doi.org/10.1016/S0016-7037(01)00886-9.
- Zheng, Y., Anderson, R.F., van Geen, A., Kuwabara, J., 2000. Authigenic molybdenum formation in marine sediments: a link to pore water sulfide in the Santa Barbara Basin. Geochem. Cosmochim. Acta 64, 4165–4178. https://doi.org/10.1016/ S0016-7037(00)00495-6.
- Zhong, Y., 2015. Study on the Depositional Age and Provenance of the Bayan Obo
- Group in the Northern Margin of North China: Implications for the Mesoproterozoic Basin Evolution of the North China Craton. Institute of Geology and Geophysics, Chinese Academy of Sciences, Beijing (in Chinese with English abstract).
- Zhu, B., Jiang, S.-Y., Yang, J.-H., Pi, D., Ling, H.-F., Chen, Y.-Q., 2014. Rare earth element and SrNd isotope geochemistry of phosphate nodules from the lower Cambrian Niutitang Formation, NW Hunan Province, South China. Paleogeogr. Paleoclimatol. Paleoecol. 398, 132–143. https://doi.org/10.1016/j.palaeo.2013.10.002.